

Review

# Three-Dimensional Heteroatom-Doped Nanocarbon for Metal-Free Oxygen Reduction Electrocatalysis: A Review

Dongbin Xiong <sup>1,2</sup>, Xifei Li <sup>2,3,\*</sup>, Linlin Fan <sup>2</sup> and Zhimin Bai <sup>1,\*</sup>

<sup>1</sup> Beijing Key Laboratory of Materials Utilization of Nonmetallic Minerals and Solid Wastes, National Laboratory of Mineral Materials, School of Materials Science and Technology, China University of Geosciences, Beijing 100083, China; xiong\_db@163.com

<sup>2</sup> Institute of Advanced Electrochemical Energy, Xi'an University of Technology, Xi'an 710048, China; tiantangzuoguai217@163.com

<sup>3</sup> Tianjin International Joint Research Centre of Surface Technology for Energy Storage Materials, College of Physics and Materials Science, Tianjin Normal University, Tianjin 300387, China

\* Correspondence: xfli@xaut.edu.cn (X.L.); zhimibai@cugb.edu.cn (Z.B.); Tel.: +86-180-0927-5876 (X.L.); +86-136-9111-5187 (Z.B.)

Received: 12 June 2018; Accepted: 27 June 2018; Published: 29 June 2018



**Abstract:** The oxygen reduction reaction (ORR) at the cathode is a fundamental process and functions a pivotal role in fuel cells and metal–air batteries. However, the electrochemical performance of these technologies has been still challenged by the high cost, scarcity, and insufficient durability of the traditional Pt-based ORR electrocatalysts. Heteroatom-doped nanocarbon electrocatalysts with competitive activity, enhanced durability, and acceptable cost, have recently attracted increasing interest and hold great promise as substitute for precious-metal catalysts (e.g., Pt and Pt-based materials). More importantly, three-dimensional (3D) porous architecture appears to be necessary for achieving high catalytic ORR activity by providing high specific surface areas with more exposed active sites and large pore volumes for efficient mass transport of reactants to the electrocatalysts. In this review, recent progress on the design, fabrication, and performance of 3D heteroatom-doped nanocarbon catalysts is summarized, aiming to elucidate the effects of heteroatom doping and 3D structure on the ORR performance of nanocarbon catalysts, thus promoting the design of highly active nanocarbon-based ORR electrocatalysts.

**Keywords:** oxygen reduction reaction; heteroatom doping; metal-free catalysts; nanocarbon; three-dimensional

## 1. Introduction

With the increasing energy consumption and environmental issues, there has been an urgent demand for the development of renewable and sustainable energy storage and conversion technologies [1–3]. Among the various technologies, rechargeable batteries, electrochemical capacitors, and fuel cells are recognized as the most efficient and feasible choices, particularly for electronic and transportation applications [4–6]. Compared with other batteries, such as nickel–metal hydride, lead–acid, and lithium–ion batteries, fuel cells and metal–air batteries have the higher theoretical energy density and higher efficiency with low emission of pollutants due to the direct conversion of chemical energy to electrical energy through chemical reaction [7–9]. For example, the typical fuel cell with H<sub>2</sub> as the fuel, O<sub>2</sub> as the oxidizing agent, and water as the end product with zero emissions and high efficiency, has drawn much attention in terms of fundamentals and applications [10,11]. However, the practical application of such fuel cells is largely restricted by the high activation barriers of electrochemical process, especially for the sluggish oxygen

reduction reaction (ORR) kinetics at the cathode [12,13]. The cathodic ORR is much slower than the anodic oxidation reaction and therefore greatly limits the output performance of these promising technologies [14]. Fortunately, electrocatalysts can play an important role to lower the activation energy barriers of the sluggish ORR. Nowadays, platinum (Pt)-based materials are considered as the most efficient ORR electrocatalysts for their excellent catalytic performance with relatively high current density and low overpotential [15–18]. However, the large-scale application of Pt-based electrocatalysts is severely hindered by the drawbacks of high cost, fuel crossover effect, instability due to CO deactivation, and Pt dissolution. Thus, it is highly urgent to develop advanced non-precious metal or even metal-free catalysts to substitute Pt-based catalysts with high catalytic activity, enhanced durability, and satisfactory cost in the long term.

Recently, much effort has been devoted to developing a series of non-precious metal ORR catalysts, such as transition metal oxides, chalcogenides, and transition metal–nitrogen–carbon (M–N/C, M = Fe, Co, Ni, Mn, etc.) materials [19–22]. However, these non-precious metal-based catalysts have some disadvantages, such as low catalytic activity compared to Pt/C and poor durability caused by the metal leaching during usage. On the other hand, metal-free carbon-based catalysts have achieved great development due to their outstanding catalytic ORR performance, high chemical stability, relatively low cost, and environmental friendliness during the past decades [23–26]. Since the first accomplishment of vertically aligned nitrogen-doped carbon nanotubes (VA-NCNTs) as metal-free ORR catalysts reported by Dai's group [27], various heteroatom-doped nanocarbon materials—such as graphene, carbon nanotubes, porous carbon, and their hybrids—have been extensively exploited as substitutes for Pt-based catalysts [28–31]. Most of the heteroatom-doped nanocarbon materials exhibit comparable or even better catalytic activity to Pt-based catalysts due to the doping-induced charge redistribution, which can facilitate the chemisorption of O<sub>2</sub> and electron transfer for the ORR process [32]. More importantly, the metal-free catalysts of doped nanocarbon materials surprisingly exhibit efficient catalytic activity and long-term stability without CO deactivation and fuel crossover effects. Therefore, developing advanced and low-cost heteroatom-doped metal-free nanocarbon materials with superior ORR catalytic activities is highly desired.

Besides the heteroatom-doping (e.g., N, S, P, B, etc.), structure engineering of nanocarbon is also a crucial strategy to determine the catalytic ORR performance, considering that the high surface area and suitable pore structure of a superior electrode configuration are the prerequisites in ensuring accessible active sites and efficient transport of electrons and ions [33–35]. For instance, engineering 3D porous structure of nanocarbon materials is a feasible approach to improve the ORR performance by providing better electrolyte permeability, electron-transfer path, and mass transport/diffusion. In recent years, for example, the fast development of nanocarbon materials (e.g., graphene) enables them to play an important role in the improvement of metal-free ORR catalysts performance [36], but 2D graphene sheets are readily to restack, which would block the active sites of catalysts and increase the resistance for mass transfer, leading to poor catalytic properties. Hence, 3D structured nanocarbon materials (cross-linked CNTs, 3D graphene, porous carbon, etc.) with chemical doping assuredly hold great prospect as efficient ORR catalysts to replace noble-metal-based catalysts [37–39].

Several reviews have been published in the past few years regarding the design of heteroatom-doped carbon nanomaterials and their applications in ORR [31,40–42]. However, special attention has not been paid to these heteroatom-doped carbon nanomaterials from the standpoint of structural effects on ORR performance. As shown in Figure 1, in this review, the current widely accepted mechanisms for ORR is briefly introduced, the recent rational design of different 3D doped-nanocarbon materials, such as 3D CNTs nanostructures, 3D graphene, porous carbon, and their hybrids is discussed as well, and then we focus on the recent achievements of 3D doped-nanocarbon materials and their enhanced ORR performance. The structure-dependent ORR performance of 3D doped-nanocarbon are well discussed, which will be beneficial to future development of non-precious metal electrocatalysts with both exceptional activity and durability in the near future.

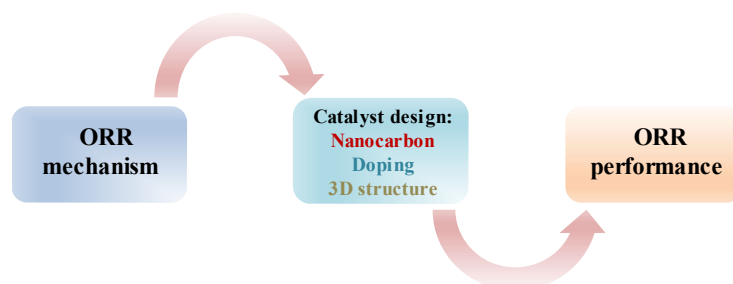


**Figure 1.** The relationships between ORR mechanism, catalyst design, and ORR performance.

## 2. The Mechanisms for ORR

The ORR is a fundamental reaction and a major limiting factor of performance for metal–air batteries and fuel cells [7,11]. In general, ORR, which involves multiple electrochemical reactions, can proceed either a four-electron path to directly produce  $\text{H}_2\text{O}$  (in acidic medium,  $4\text{H}^+ + \text{O}_2 + 4\text{e}^- \rightarrow 2\text{H}_2\text{O}$ ) and  $\text{OH}^-$  (in alkaline medium,  $2\text{H}_2\text{O} + \text{O}_2 + 4\text{e}^- \rightarrow 4\text{OH}^-$ ) as the final products or a less efficient two-step two-electron pathway with the formation of  $\text{H}_2\text{O}_2$  (in acidic medium,  $\text{O}_2 + 2\text{H}^+ + 2\text{e}^- \rightarrow \text{H}_2\text{O}_2$ ,  $\text{H}_2\text{O}_2 + 2\text{H}^+ + 2\text{e}^- \rightarrow 2\text{H}_2\text{O}$ ) or  $\text{HO}_2^-$  (in alkaline media,  $\text{O}_2 + \text{H}_2\text{O} + 2\text{e}^- \rightarrow \text{HO}_2^- + \text{OH}^-$ ,  $\text{HO}_2^- + \text{H}_2\text{O} + 2\text{e}^- \rightarrow 3\text{OH}^-$ ) as the intermediate specie [41,43]. As schematically shown in Figure 2, in a typical proton exchange membrane fuel cell (PEMFC), hydrogen and oxygen/air continuously enter the anode and the cathode, respectively [44]. The fuel molecules ( $\text{H}_2$ ) are oxidized at the anode ( $\text{H}_2 \rightarrow 2\text{H}^+ + 2\text{e}^-$ ). In this process, the electrons flow out of the anode to provide electrical power, while protons diffuse across the electrolyte membrane towards the cathode and react with adsorbed oxygen to produce water (ORR,  $4\text{H}^+ + \text{O}_2 + 4\text{e}^- \rightarrow 2\text{H}_2\text{O}$ ). The ORR occurs by efficient four-electron reduction.

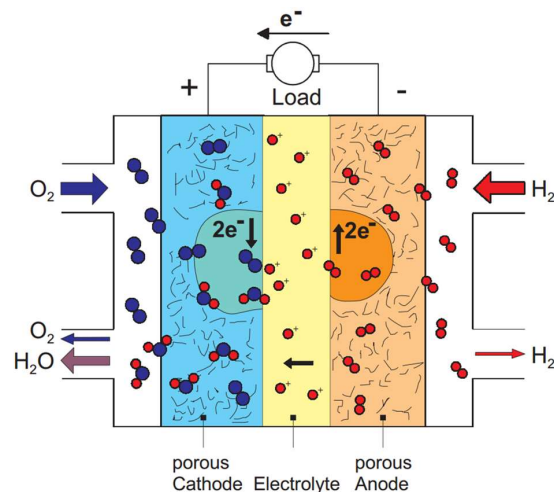


**Figure 2.** Schematic illustration of a hydrogen/oxygen fuel cell and its reactions based on the PEMFC. Reproduced from [44], Copyright 2001, Wiley.

Generally, the four-electron reduction mechanism is favorable for ORR owing to its efficiency advantage and the avoiding of hydrogen peroxide intermediate species that can damage the membrane and ionomer [45]. However, the ORR at the cathode suffers from complicated electron transfers, as illustrated in Figure 3, in a full reduction pathway (Figure 3a), the O–O bond of adsorbed  $\text{O}_2$  breaks into two  $\text{O}^*$  intermediates which could be reduced to  $\text{OH}^-$  and  $\text{H}_2\text{O}$  as the final products in the alkaline and acidic conditions, respectively. While for partial reduction to take place, as shown in Figure 3b,  $\text{O}_2$  is first adsorbed on to the catalyst surface, then the adsorbed  $\text{O}_2$  couples two protons to form  $\text{HOOH}^*$  intermediates before the O–O bond is cleaved, leading to a high yield of  $\text{H}_2\text{O}_2$  or  $\text{HO}_2^-$  via a two-electron pathway, which should be avoided during the ORR process [46,47].

Under acidic conditions, the ORR is inherently several orders of magnitude slower than the HOR, and catalysts are required to lower activation barriers of the sluggish ORR. Only a few types of materials, to date, have been found to provide suitable activity and stability towards the ORR in acidic media, such as heteroatom-doped nanocarbon materials and the transition metal-based NP functionalized carbon nanomaterials [21,48]. While the ORR kinetics are more favorable in alkaline mediums, providing an opportunity to use non-precious metal catalysts, such as metal-oxides and doped nanocarbon materials [45].

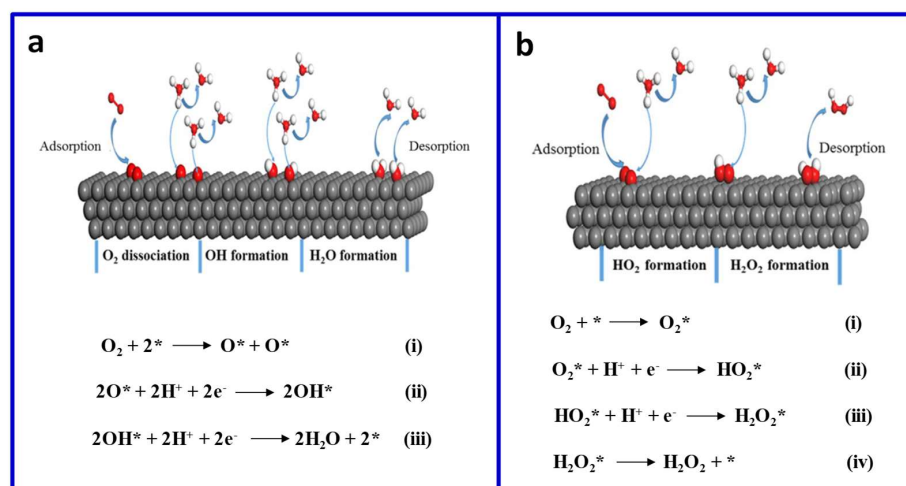


**Figure 3.** Proposed mechanism schematics of (a) full reduction and (b) partial reduction of oxygen. Reproduced from [47], Copyright 2016, Elsevier.

### 3. 3D Heteroatom-Doped Nanocarbon Electrocatalysts for ORR

Carbon materials, especially nanostructured carbons, has been widely used as electrode materials for energy storage and conversion devices originating from their general advantages, such as good conductivity for rapid electron transfer, super large active surface area for ion adsorption, and superior chemical stability for resistance of acid and alkaline corrosion [33,49–51]. Additionally, the tailorable surface chemistry, abundant structural variety, and low cost of nanocarbons together boost their harvesting as active catalysts for ORR in metal–air batteries and fuel cells [22,34]. Nevertheless, structure optimization of nanocarbon catalysts is one of the main strategies to sufficiently expose and/or activate the catalytic sites. It is noted that low-dimensional nanocarbons—including 0D fullerene, 1D carbon nanotubes, and 2D grapheme—usually have low utilization efficiency due to the embedded active sites on the limited surface, which is unfavorable for both mass transport and electron transfer during ORR process [33,52]. However, when fabricated to be a continuous 3D porous structure, the 3D nanocarbon can provide a high surface area with abundant exposed active sites, contributing to good electrocatalytic performance. More importantly, the 3D nanostructures play a critical role in greatly accommodating discharge products and providing channels for ion transfer and oxygen diffusion, further accelerating reaction kinetics [53].

Over the past decade, carbon-based metal-free electrocatalysts doped with heteroatom, such as N, S, B, P, and their mixtures, have emerged as front runners to replace Pt and other noble metals for highly efficient ORR [22,54]. Both experiments and theoretical calculations show that the doping of heteroatoms in the sp<sup>2</sup> lattice of graphitic carbon can alter the electronic arrangement of the carbon-based material and tailor their electron donor properties, as a result, breaking the electroneutrality of sp<sup>2</sup> carbon to create charged sites favorable for O<sub>2</sub> adsorption and enhancing effective utilization of carbon π electrons for O<sub>2</sub> reduction, thus leading to improved ORR electrocatalytic activity [24,29,43]. Despite the great improvements that have been achieved, most of the carbon-based metal-free catalysts still show inferior intrinsic ORR activities compared with Pt-based ones though with better stability and lower costs. Increasing evidences

profile that efficient ORR nanocarbon catalysts should be favored to have abundant accessible active sites for implementing reaction, good conductivity for charge transfer, and suitable porous structure for mass transport. The presence of adequate reactive sites in combination with novel structural design makes them attractive metal-free catalysts. To achieve the aforementioned merits, various heteroatom-doped 3D nanocarbon materials, such as N-doped CNT aerogels [37], nanoporous N-doped graphene [55], N, P-doped porous carbon, and doped graphene/CNT hybrid materials have been developed as high-performance ORR catalysts (Figure 4) [56,57].

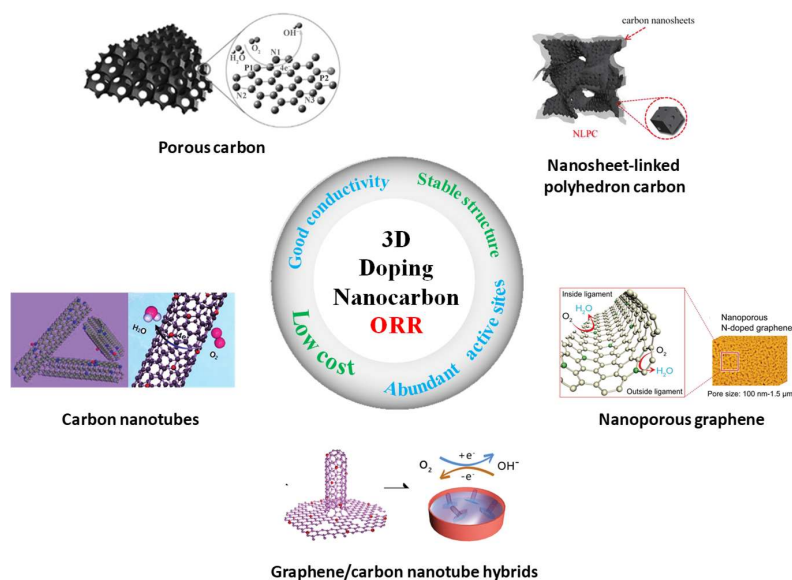


**Figure 4.** Advantages of metal-free 3D doped-nanocarbon materials and their applications as high-efficiency ORR electrocatalysts.

### 3.1. Heteroatom-Doped 3D CNTs for ORR

As typical 1D  $sp^2$ -hybridized carbon nanomaterials, CNTs can be considered as 2D graphene sheets rolled up into nanoscale tubes [8,58]. Because of their unique structural characteristics and outstanding physicochemical properties—such as large surface area, high mechanical property, good electrical conductivity, and excellent chemical stability—CNTs have stimulated continuous interest in the field of nanotechnology, especially in environmental and energy areas, in recent decades [52,59]. When heteroatoms are appropriately doped into the carbon matrix of CNTs, enhanced ORR performance can be achieved [8]. Doped-CNTs function in enhancing electrical conductivity, oxygen mass transfer, corrosion resistance, and water removal of catalysts, leading to improved catalytic activity and durability [60,61]. More importantly, putting the tiny cylindrical nanotubes together into an integral 3D framework with interconnection and rational distribution and controlling the porous structure can provide abundant exposed active sites and stable electron/mass transport skeleton, and hence ORR activity [37].

#### 3.1.1. Single Heteroatom-Doped 3D CNTs

In 2009, Dai et al. synthesized N-doped VA-CNTs through pyrolyzing iron(II) phthalocyanine (FePc) in the presence of additional  $NH_3$  gas (Figure 5a) [27]. The proposed 3D N-doped VA-CNTs were discovered to be superior to commercially Pt/C catalysts for the electrocatalysis of the ORR with a much higher catalytic activity, lower overpotential, smaller crossover sensitivity, and better long-term stability in alkaline electrolytes (Figure 5b). The catalytic mechanism of nitrogen-doped VA-CNTs for the ORR was investigated using quantum mechanical calculations based on the B3LYP hybrid density functional theory (DFT), results suggest that the introduce of nitrogen dopants changes the

charge density of carbon atoms (Figure 5c). Based on the theoretical and experimental results, Dai and co-workers presented that the N-induced charge delocalization could change the chemisorption mode of O<sub>2</sub> from the end-on adsorption (Pauling model) at the non-doped CNT surface (top, Figure 5d) to a side-on adsorption (Yeager model) onto the N-doped CNT surface (bottom, Figure 5d). Interestingly, the parallel diatomic adsorption could effectively weaken the O–O bonding to facilitate ORR at the N-doped VA-CNTs electrodes. Besides the high surface area, good electrical and mechanical properties of 3D vertically aligned CNTs provide additional advantages for the nanotube electrode in fuel cells. It should be noted that a certain amount of residual Fe catalyst herein may exist in the N-doped VA-CNTs. The metal contaminants are believed to have certain effects on ORR performance. Therefore, it is urgently needed to develop a metal-free synthesis route to produce N-doped CNTs in order to confirm the actual electroactivity of N-doped CNTs for ORR without the disturbance of metal residue.

To reveal the intrinsic catalytical mechanism of N-doped CNTs, several technologies including metal-free catalysis growth and detonation-assisted chemical vapor deposition (CVD) have been developed [62,63]. By using an erasable-promoter-assisted hydrothermal reaction coupling with pyrolysis, Zhang and co-workers synthesized clean, high-specific surface area (~869 m<sup>2</sup>·g<sup>-1</sup>), and highly conductive (~10.9 S·m<sup>-1</sup>) N-doped CNT aerogels [37]. During the synthetic process, N doping was realized by pyrolysis of aerogels with pyrrole molecules as 'built-in' nitrogen sources (post-treatment), importantly, the electrical conductivity of CNT aerogels was restored and the  $\pi$ - $\pi$  stacking between CNTs was enhanced through thermal treatment, which can repair the  $\pi$ -conjugated skeleton of CNTs, thereby maintaining the 3D gel network (Figure 5e,f). Owing to the unique structure with 3D frameworks constructed by randomly entangled CNTs, the obtained N-CNT aerogels (Figure 5g) exhibited superior activity and high stability for ORR catalysis in alkaline conditions. Moreover, the crossover test (Figure 5h) demonstrated that the N-CNT aerogels electrode efficiently inhibit the crossover effect of methanol. Zhu et al. prepared porous N-doped CNTs by activation and pyrolysis of polypyrrole nanotubes [64], which result in a hierarchical porous structure with in situ N doping. This material exhibited excellent catalytic activity with a four-electron pathway for ORR in alkaline condition. They believe that the favorable ORR activities of N-doped CNTs were attributed to its porous tube structure, high surface area, and uniform N distribution. Template method is considered as the most effective strategy for the preparation of ordered porous nanostructures. By using an anodic alumina oxide template, Yang et al. fabricated a N-doped macroporous carbonaceous nanotube array for ORR catalyst (Figure 5i,j) [65]. The nanotubes with macroporous feature can facilitate mass transfer within the electrodes. The doping of electron-rich N which can activate the p electrons of sp<sup>2</sup> carbon by conjugating with the lone-pair electrons from nitrogen dopants can provide more active sites to adsorb O<sub>2</sub>. These merits together contribute to the high performance for ORR in terms of onset potential, half-wave potential values, reaction current, and durability.

There are several different nitrogen configurations including pyrrolic N, pyridinic N, and graphitic N in carbon matrix [54]. Pyrrolic N and pyridinic N are located at the edges and bonded to two carbon atoms, while graphitic N is incorporated in the core structure of the carbon materials by replacing the sp<sup>2</sup>-hybridized carbon atom. Generally, different configurations with different N type would affect the electronic structure of neighboring carbon atoms, leading to different catalytic properties. Up to date, numerous N-doped CNT materials have been prepared via different synthetic strategies for ORR electrocatalyst [37,64,66,67]. However, it is still unclear whether the pyridinic or graphitic N is mainly responsible for the active sites for the ORR. Recent theoretical work and experiments suggest that pyridinic N improves the onset potential, whereas the graphitic N determines the limiting current density for the ORR [24]. Pyridinic N can provide one p electron to the aromatic  $\pi$  system with a lone electron pair in the plane of the carbon matrix to enhance the electron-donating capability of the catalyst. Therefore, pyridinic N can weaken the O–O bond via the bonding of O with N and/or the adjacent C atom to facilitate the reduction of O<sub>2</sub>.

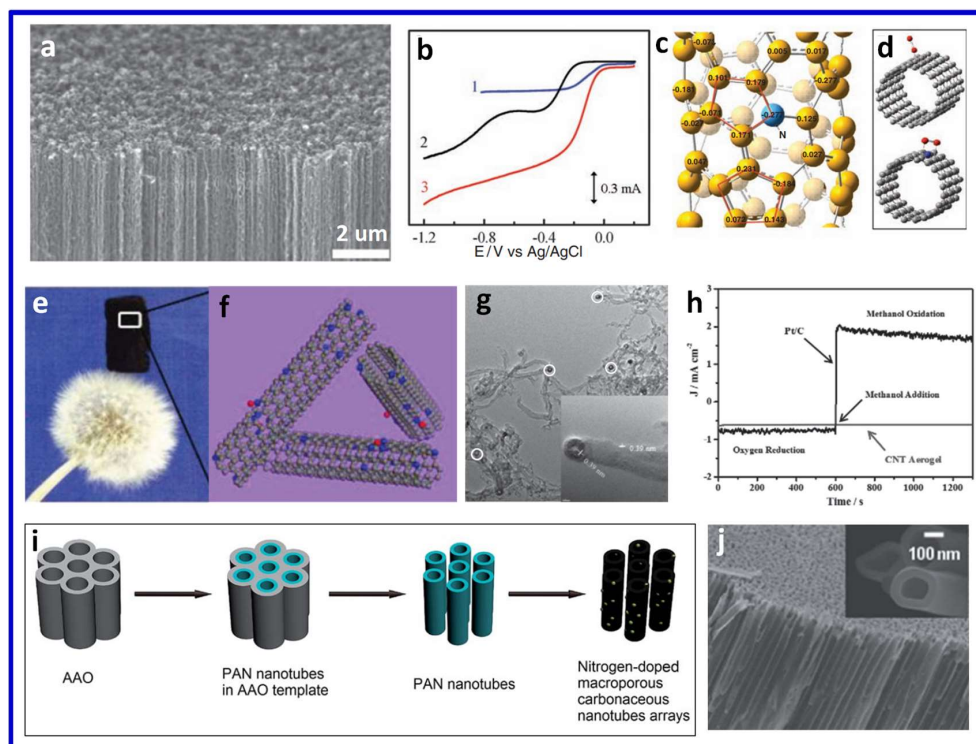


**Figure 5.** (a) Scanning electron microscopy (SEM) image of N-doped VA-CNTs; (b) ORR polarization curves of Pt/C (curve 1), VA-CNTs (curve 2), and N-doped VA-CNTs (curve 3); (c) Calculated charge density distribution for the N-doped CNTs; (d) Schematic representations of possible adsorption modes of an oxygen molecule at the CNTs (top) and N-doped CNTs (bottom). Reproduced from [27], Copyright 2009, American Association for the Advancement of Science. (e) Digital photograph; (f) model schematic diagram; and (g) Transmission electron microscopy (TEM) image of N-doped CNT aerogels; (h) Methanol crossover effect measurements of N-doped CNT and Pt/C catalyst at  $-0.4$  V. Reproduced from [37], Copyright 2015, Wiley. (i) The fabrication process and (j) SEM image of N-doped macroporous carbonaceous nanotubes arrays. Reproduced from [65], Copyright 2014, The Royal Society of Chemistry.

Similar to N-doped CNTs, other heteroatom (e.g., phosphorus and boron)-doped CNTs also demonstrated improved electrocatalytic activity toward ORR, compared to its undoped counterpart [60,68]. Boron and phosphorus have a similar effect on the ORR activity as N, as they both disrupt the charge uniformity and change the charge density of the carbon network. However, the mechanisms of B-doped CNTs and N-doped CNTs are different. There are multiple active B moieties in B-doped CNTs, including  $BC_3$ ,  $B_4C$ ,  $BC_2O$ , and  $BCO_2$ . Owing to the lower electronegativity of B (2.04) than C (2.55), positively polarized B dopant in B-doped CNTs on one hand adsorbs  $O_2$  on the other hand acts as a bridge to transport electrons from graphitic carbon p electrons to  $O_2$ , which can also improve the ORR activity. Although the ORR performance of B-doped CNT materials is not competitive to that of commercial Pt/C catalyst, the proportional relationship between the boron content and ORR performance suggests the great potential of B-CNTs for further improvement. P doped-CNTs are another interesting type of metal-free catalysts for improving ORR because P has the same number of valence electrons as N and often shows similar chemical properties. For example, p-doped MCNTs were reported to exhibit much higher ORR activity than commercial Pt/C in alkaline fuel cells [69]. Very recently, Zhang and co-authors also confirmed that porous P-doped CNTs exhibit better ORR catalytic activity than that of undoped-CNTs [68].

### 3.1.2. Multiple Heteroatom-Co-Doped 3D CNTs

Addition to the single heteroatom-doped CNTs, co-doped CNTs with different heteroatom were investigated to show much better electrocatalytic ORR performance due to the synergistic effect between different heteroatoms. Vertically aligned MWCNT arrays co-doped with P atoms and N atoms were first synthesized by an injection-assisted CVD method [61]. Because of the synergistic effect arising from co-doping CNTs with both P and N, the obtained P, N co-doped MWCNT arrays significantly show outstanding electrocatalytic activity toward ORR comparable to the commercial Pt/C electrode and significantly better than that of CNTs doped by P or N only. Subsequently, another N, P-dual-doped CNT array was synthesized by a novel one-pot method with an aminophosphonic acid resin as the N, P, and C sources [70]. Compared with traditional bamboo-shaped N-CNTs and N, P-dual-doped CNTs, the as-obtained N, P-CNTs with unique architecture of which the large hollow channels and open ends provide abundant catalytic active sites in inner walls, being accessible to oxygen molecules exhibited comparable activity and much better CO and methanol tolerance towards ORR to Pt/C catalysts.

### 3.2. Heteroatom-Doped 3D Graphene for ORR

Graphene, which is composed of one monolayer of carbon atoms with a honeycomb structure, has been widely explored in different fields for its fascinating physical and chemical properties [71,72]. However, graphene is constructed of  $sp^2$ -bonded carbon atoms via hybridization of  $s$ ,  $p_x$ , and  $p_y$  atomic orbitals, resulting in a zero-band gap semiconductor with the conduction and valence bands. The lack of intrinsic bandgap muchly limits the applications of pristine graphene in the areas of energy storage, electrocatalysis, and nanoelectronics [73]. Fortunately, chemical doping with foreign atoms has been demonstrated to be an effective method to tailor the electronic and electrochemical properties of graphene by changing the electronic density within the graphene sheet, thus opening the bandgap in graphene, and extending its applications [74,75]. For example, the increased active sites and enhanced catalytic activity of graphene towards ORR have been achieved by doping with foreign non-metallic atoms (e.g., N, B, P, or S) [36,76–78].

Other than heteroatom doping, morphology control, and structural design, which relate to the surface area, pore structure and electron donating/withdrawing capability, is perhaps the most effective way to enhance the ORR activity of graphene materials [29,33]. Especially, heteroatom doping, in company with 3D structure design, has been a popular and widely accepted strategy to develop graphene-based ORR electrocatalyst [79–82].

#### 3.2.1. Single Heteroatom-Doped 3D Graphene

After their first discovery of metal-free VA-NCNTs as high-performance ORR electrocatalysts, Dai et al. used a modified CVD method to prepare N-doped graphene films on Ni-coating  $SiO_2/Si$  substrate [83]. They demonstrated that the N-graphene can act as a metal-free catalyst with a much better catalytic activity, tolerance to crossover effect, and long-term stability than Pt catalyst for ORR via a four-electron pathway in alkaline fuel cells. Subsequently, N-doped graphene was synthesized via catalyst-free thermal annealing graphite oxide and nitrogen source [76]. The synthesized N-doped graphene materials, which completely avoid the contamination of metal catalysts, have high nitrogen content and exhibit excellent catalytic activities toward ORR in alkaline electrolytes.

3D graphene structures can effectively restrain the restacking between graphene sheets, and therefore expose more active sites, heteroatom-doped 3D graphene materials are expected to show much better electrocatalytic performance for ORR than the 2D ones [84,85]. By using a hydrothermal self-assembly approach followed by high-temperature treatment, as shown in Figure 6a, Qiu et al. fabricated 3D porous N-doped graphene aerogels (NPGAs, Figure 6b), which exhibited good electrocatalytic activity and long-term stability in a  $Li-O_2$  cell system [86]. The large void volume, interconnected porous channels, multidimensional electron transport pathways, less stacking of graphene sheets and the sufficient exposure

of active sites originated from the doped N atoms within graphene sheets collectively contribute to the outstanding electrochemical performances of the as-made NPGA. Yi et al. prepared highly conductive and ultralight nitrogen-doped graphene nanoribbons aerogel (N-GNRs-A) by using a facile hydrothermal method (Figure 6c) [81]. Due to the synergistic effect of the nanoporous structure, high surface area, good conductivity and the N-doped structural integrity of the GNRs, the proposed aerogel as a novel ORR catalyst show comparable catalytic activity (Figure 6d), superb methanol tolerance (Figure 6e), and better stability (Figure 6f) than commercial Pt/C catalysts in both alkaline and acidic solutions. After that, various 3D N-doped graphene materials prepared through different methods have been developed as high-performance ORR catalysts [38,86–88]. S-doped 3D porous RGO hollow nanospheres framework (S-PGHS), prepared with GO and dibenzyl disulfide as precursors, exhibited superior electrocatalytic activity comparable with that of commercial Pt/C (40%), and much better durability and methanol tolerance [89]. 3D sulfur-doped graphene networks S-GFs were also prepared by using an ion-exchange/activation combination method, which showed outstanding ORR catalytic performance [90]. Recently, 3D P-doped graphene (3DPG) fabricated by CVD method with nickel foam as template and triphenylphosphine (TPP) as C and P sources was proposed as ORR catalyst, which exhibited better catalytic activity, long-term stability, and methanol tolerance than pristine 3D graphene and commercial Pt/C [91].

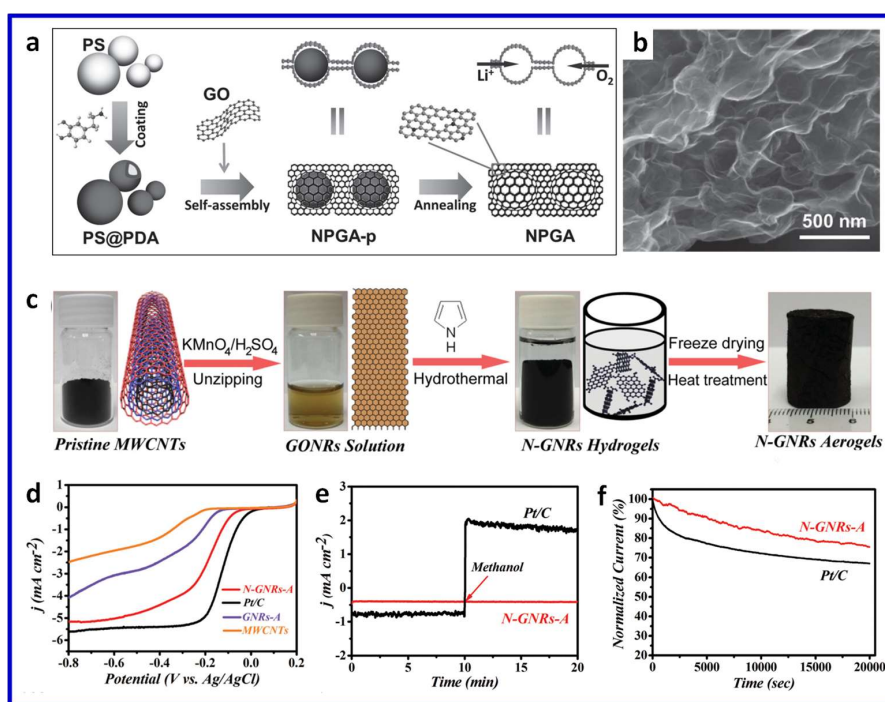


**Figure 6.** (a) Schematic process for synthesis of 3D NPGAs; (b) SEM image of 3D NPGAs. Reproduced from [86], Copyright 2015, Wiley. (c) Illustration of the synthetic route for N-GNRs-A; (d) Linear sweep voltammetry (LSV) curves of pristine MWCNTs, GNRs-A, N-GNRs-A, and Pt/C in an  $O_2$ -saturated 0.1 M KOH solution at a scan rate of  $10 \text{ mV s}^{-1}$  and a rotation speed of 1600 rpm; (e) Methanol crossover effect on N-GNRs-A and Pt/C upon addition of 3 M methanol after about 10 min in an  $O_2$ -saturated 0.1 M KOH solution at  $-0.4 \text{ V}$ ; (f) Current–time chronoamperometric response of N-GNRs-A and Pt/C catalysts at  $-0.4 \text{ V}$  in  $O_2$  saturated 0.1 M KOH aqueous solution at a rotation rate of 1600 rpm. Reproduced from [81], Copyright 2014, Wiley.

### 3.2.2. Multiple Heteroatom-Co-Doped 3D Graphene

Co-doped 3D graphene has been expected to possess better electrocatalytic performance compared to single doped 3D graphene due to the synergistic effect between different heteroatoms. Qiao and co-authors prepared N and S dual-doped mesoporous graphene (N-S-G) for the first time as a metal-free

catalyst for ORR [92]. The obtained N-S-G showed outstanding ORR performance, which is comparable to commercial Pt/C and prominently better than that of graphene catalysts doped solely with S or with N. Furthermore, by using further DFT calculations, they elucidated that the synergistic performance improvement results from the redistribution of spin and charge densities caused by the co-doping of S and N, which leads to abundant carbon atom active sites. Soon after that, 3D N, S co-doped graphene frameworks (N/S-GFs) and 3D B, N co-doped graphene foams (BN-GFs) were prepared by one-pot hydrothermal approach and modified CVD method, respectively [79,80]. Both of which manifested superior ORR catalytic behavior with mainly four-electron transfer pathway in alkaline condition. 3D N, B-doped graphene aerogels (N, B-GAs) prepared via a two-step method involves a hydrothermal reaction and a pyrolysis procedure were also demonstrated to exhibit an outstanding catalytic activity for the ORR [93]. Among the dual-doped 3D graphene materials for ORR catalysts, N, S co-doped 3D graphene is the most popular one and has been widely prepared by various methods including biomass pyrolysis [94], hydrothermal method [95,96], hydrothermal reaction-pyrolysis two-step method [97], and soft template-assisted method [98].

In addition to dual doping, co-doping 3D graphene catalysts with more than two different heteroatoms is also an effective strategy to enhance the ORR performance, as exemplified by N-P-O co-doped 3D graphene [99]. The N-P-O co-doped free-standing 3D hierarchical porous graphene (3D-HPG) was fabricated through a one-pot gas-exfoliation assisted ‘cutting-thin’ technique from solid carbon sources (Figure 7a). The produced graphene exhibited continuously 3D hierarchical porous structure with heteroatoms of N, P, and O simultaneously doped into the carbon frameworks, which can effectively modulate the electronic characteristics and surface chemical feature (Figure 7b). The resultant N-P-O co-doped 3D-HPG catalysts exhibited excellent ORR activity. As shown in Figure 7c, in a 0.1 M KOH electrolyte, the ORR polarization curves reach well-defined diffusion limiting currents, and the Koutecky–Levich (K–L) plots suggest the good linearity at varied potentials with the electron transfer number calculated to be 3.83, which is comparable to the commercial Pt/C catalyst. Significantly, the durability of N-P-O co-doped 3D-HPG is much better than that of commercial Pt/C catalyst (Figure 7d).

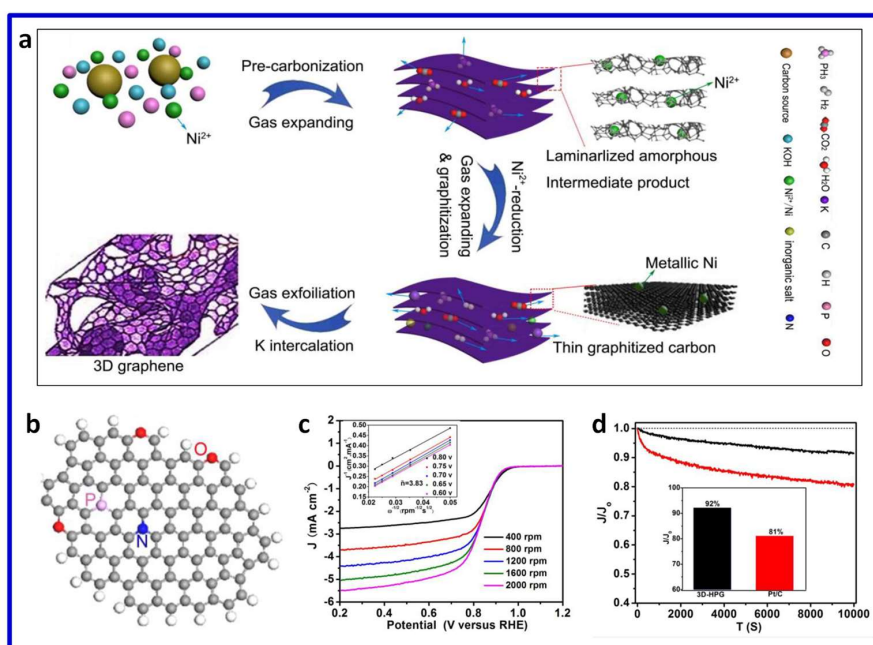


**Figure 7.** (a) Schematic process for synthesis of N-P-O co-doped 3D-HPG; (b) Schematic model of 3D-HPG; (c) ORR polarization curves for 3D-HPG at different rotating rates in O<sub>2</sub>-saturated 0.1 M KOH solution at scanning rates of 5 mV·s<sup>-1</sup>, inset: K–L plots; (d) The current vs. time (i-t) chronoamperometric responses of 3D-HPG and Pt/C in O<sub>2</sub>-saturated 0.1 M KOH at a constant potential at 0.65 V (versus RHE) and a rotation rate of 1600 rpm, inset: the ratio of the J/J<sub>0</sub>. Reproduced from [99], Copyright 2016, Elsevier.

### 3.3. Heteroatom-Doped 3D Porous Carbon for ORR

Engineering a 3D porous structure—which can provide good electrolyte permeability, mass transport, and an electron-transfer path—is considered the most promising approach to enhance the ORR performance of carbon-based non-precious metal ORR electrocatalysts. Up to now, various 3D porous carbon materials have been exploited as promising and efficient catalysts for their outstanding virtues such as low cost, high conductivity, high surface area with abundant porosity, designable carbon framework, as well as high chemical and mechanical stability [100–103]. Similar to 3D CNTs and 3D graphene, 3D porous carbon can also be doped with heteroatoms for ORR electrocatalysts [104].

#### 3.3.1. Single Heteroatom-Doped 3D Porous Carbon

To develop N-doped carbon materials without any metal components, Feng and co-workers fabricated N-doped 3D ordered mesoporous carbons (N-OMCs) via a metal-free nanocasting technology by using SBA-15 as the template and *N,N'*-bis(2,6-diisopropylphenyl)-3,4,9,10-perylenetetracarboxylic diimide (PDI) as the precursors [100]. Owing to its high surface area and a graphitic framework with an appropriate nitrogen content, the obtained N-OMCs exhibited outstanding ORR performance with high catalytic activity, efficient resistance to crossover effects and excellent long-term stability. The ORR performance was superior to that observed for the commercial Pt/C catalyst, suggesting the superior ORR activity of N-OMCs. Soon after that, another nitrogen-doped carbon nanocages (NCNCs) with high nitrogen content and specific surface area were prepared by using in situ generated MgO as a template and pyridine as the source of both carbon and nitrogen [105]. The resulting NCNCs exhibited superior ORR performance with outstanding stability towards methanol crossover and CO poisoning in alkaline solution. Importantly, without the interference of metal impurities, this study clarifies that it is the N-doped carbon species rather than the metal-related active sites are responsible for the ORR activity of the NCNCs. By using a green biomass source method with fermented rice as starting materials, Qu and co-authors fabricated a porous N-doped carbon spheres (N-CSs) with high specific surface areas ( $2105.9 \text{ m}^2 \cdot \text{g}^{-1}$ ) and high porosity ( $1.14 \text{ cm}^3 \cdot \text{g}^{-1}$ ) [106]. When tested as ORR catalyst for fuel cells, the proposed N-CSs exhibit excellent catalytic activity with long-term stability and good resistance to crossover effects and CO poisoning superior to that of the commercially available catalyst Pt/C. Later, various N-doped 3D porous carbon derived from different biomass—such as malachium aquaticum [107], shrimp-shell [108], and porous cellulose [109]—have been demonstrated to exhibit excellent ORR performance.

In general, two crucial factors—including the doped element content/type and specific surface area/porous structure—govern the performance of the carbon-based ORR catalysts. Recently, to simultaneously optimize both surface functionalities and porous structures of the metal-free catalysts, Feng et al. developed N-doped carbon materials by using templating synthesis with nitrogen-enriched aromatic polymers as precursors and subsequent  $\text{NH}_3$  activation (Figure 8a) [102]. The as-fabricated nitrogen-doped mesoporous carbon exhibit the outstanding ORR activity in alkaline media with half-wave potential of 0.85 V versus reversible hydrogen electrode with a loading of  $0.1 \text{ mg} \cdot \text{cm}^{-2}$ . More importantly, the  $\text{H}_2\text{O}_2$  yield measured with meso/micro- $\text{P}_0\text{PD}$  remained below 5% at all potentials, corresponding to a favorable high electron-transfer number of 3.97 (Figure 8b). Superior electrochemical durability was also observed for the meso/micro- $\text{P}_0\text{PD}$  to the Pt/C catalyst under the same condition (Figure 8c). It should be noted that most N atoms are buried within the N-doped carbons, and these hidden N atoms are inaccessible to the reactants during ORR process. Recently, Wang and co-workers developed a 3D N-doped hierarchical porous carbon monolith (NHPCM) composed of branched mesoporous rods via an in situ source-template-interface reaction route by using furfuryl alcohol as the carbon source (Figure 8d) [103]. Owing to the increased exposure and achievability of the catalytic sites originates from the favorably activated  $\text{O}_2$  at the edged groups, the resulting hybridized carbon nanowires possess an outstanding electrocatalytic ORR activity with a four-electron dominant reaction pathway. Interestingly, in spite of low N content, the NHPCM with 1.1 at% N shows not only superior ORR activity, but also improved MeOH crossover and high durability compared to commercial Pt/C (Figure 8e,f). This phenomenon is ascribed to the high ratio of graphitic to pyridinic N and the unique 3D macroporous scaffold with interconnected mesoporous rods,

as well as the easily reachable catalytic sites. Uninterruptedly, various N-doped 3D porous carbon materials were exploited for ORR catalysts [110–115].

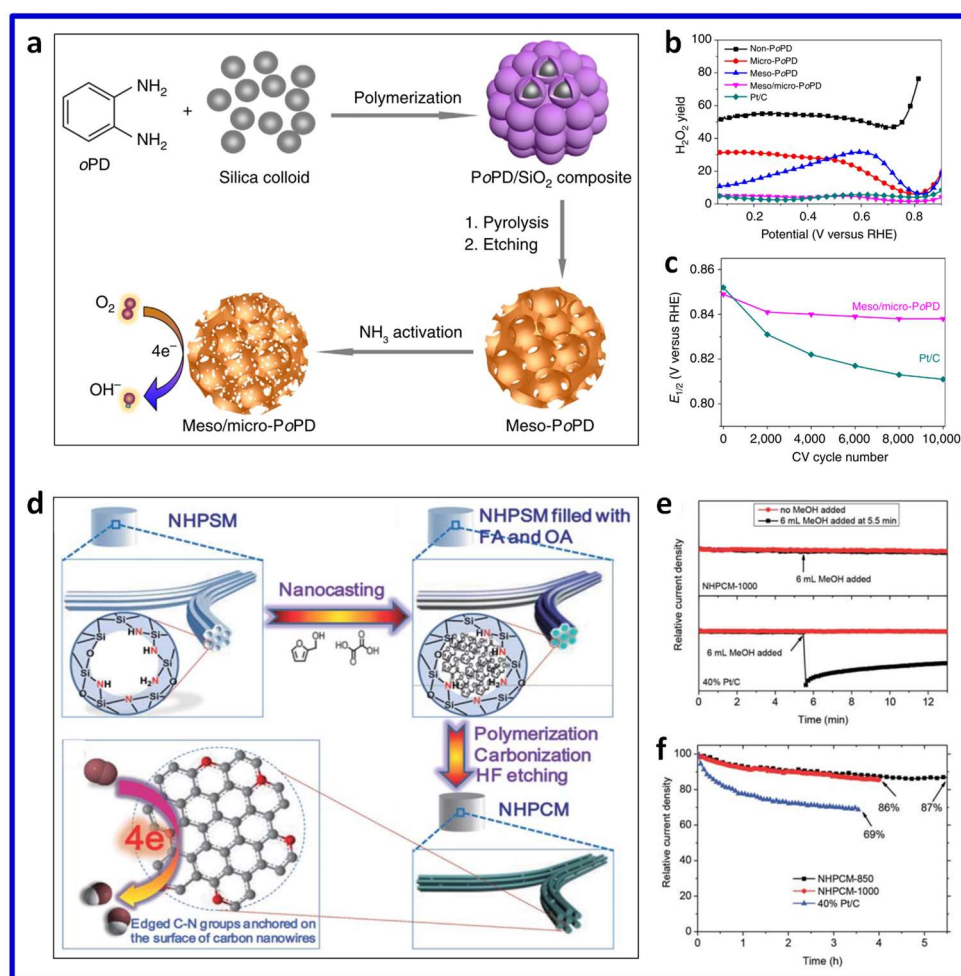


**Figure 8.** (a) Schematic illustration of the synthesis of meso/micro-N-doped carbon (P<sub>0</sub>PD) electrocatalyst; (b) H<sub>2</sub>O<sub>2</sub> yields plots of meso/micro-P<sub>0</sub>PD, reference materials, and Pt/C catalyst; (c) Half-wave potential of meso/micro-P<sub>0</sub>PD and Pt/C with the same loading of 0.1 mg cm<sup>-2</sup> as a function of the number of potential cycles in O<sub>2</sub>-saturated electrolyte. Reproduced from [102], Copyright 2014, Macmillan Publishers Limited; (d) Schematic illustration of the synthesis of 3D N-doped hierarchical porous carbon monolith (NHPCM) electrocatalyst; (e) Current-time chronoamperometric response of NHPCM-1000 and Pt/C with or without the addition of 6 mL MeOH into the electrochemical cell containing 100 mL electrolyte at 0.6 V (vs. RHE) with a rotating rate of 1600 rpm; (f) Current-time chronoamperometric response of NHPCM-850, NHPCM-1000, and Pt/C over 3.5 h at 0.6 V (vs. RHE) in O<sub>2</sub>-saturated 0.1 M KOH solution at 1600 rpm. Reproduced from [103], Copyright 2015, Wiley.

### 3.3.2. Multiple Heteroatom-Co-Doped 3D Porous Carbon

As described above, the synergistic effect arising from the co-doping of heteroatoms significantly enhances the ORR activity of metal-free catalysts. For example, a 3D sulfur–nitrogen co-doped carbon foams (S–N–CF) with hierarchical pore structures were demonstrated to show better ORR performance with higher catalytic activity, higher methanol tolerance and longer-term stability than a commercial Pt/C catalyst [101]. The relationship between the catalyst properties and structures of metal-free carbon materials for ORR was also clarified: (1) the high heteroatom doping for S–N–CF can provide abundant active sites; (2) the hierarchical pore structures and 3D networks can ensure fast electron

transfer and reactant transport within the electrodes. More recently, multiple heteroatom-co-doped 3D porous carbons—such as 3D S–N co-doped carbon foams [101], N and P dual-doped hierarchical porous carbon foams [39]; B, N co-doped 3D porous graphitic carbon [116]; N and P co-functionalized 3D porous carbon networks [117]; and N, S, and O co-doped hierarchically porous carbon [118]—have been developed as efficient metal-free electrocatalysts for ORR. As an example, the N, S, and O co-doped hierarchically porous carbon were fabricated via a one-pot pyrolysis reaction with silica as template, sucrose and trithiocyanuric acid (TA) as precursors [118]. A hierarchically micro-, meso-, and macroporous carbon featured with abundant dopant species and high specific surface area were obtained (Figure 9a). The resulting product displays abundant low contrast holes with diverse sizes, suggesting the featured hierarchical porosity (Figure 9b). When tested in acidic electrolytes, the one-pot pyrolyzed metal-free electrocatalysts with optimized structure exhibits comparable or even better ORR activities than the commercial Pt/C catalyst (Figure 9c,d). The excellent electrocatalytic performance is ascribed to the abundant dopant species, good integrated conductivity, and hierarchically porous architecture.

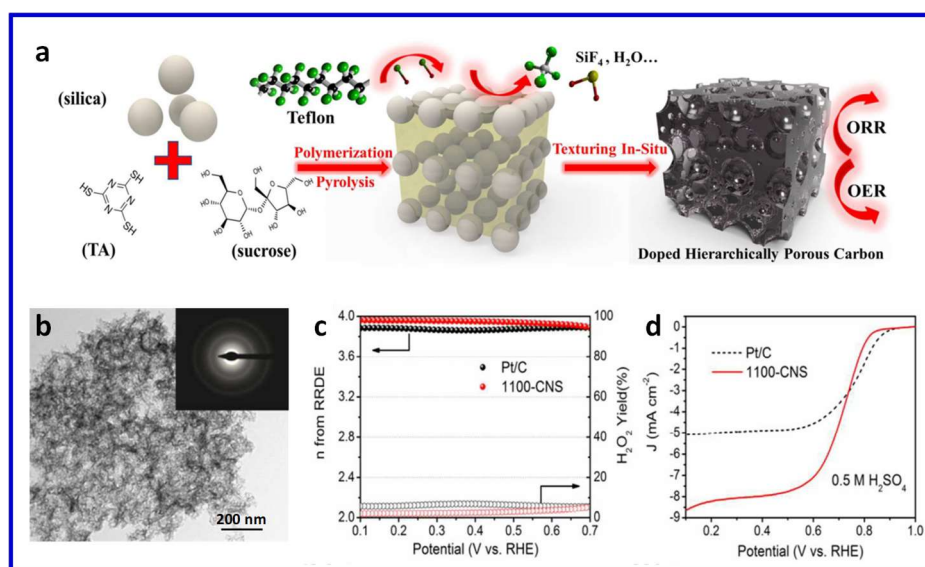


**Figure 9.** (a) Illustration of the one-pot fabrication process of N, S-doped porous carbon (CNS) materials; (b) TEM observation of the CNS sample, inset is the SAED patterns; (c) RRDE voltammograms of the 1100-CNS and Pt/C samples at 1600 rpm; (d) Electron transfer number ( $n$ ) and  $\text{HO}_2^-$  yield derived from the RRDE test. Reproduced from [118], Copyright 2017, The Royal Society of Chemistry.

### 3.4. Nanocarbon Hybrid Materials for ORR

In addition to heteroatom-doped 3D CNT, graphene and porous carbon nanomaterials discussed above, nanocarbon hybrid materials with 3D structures also show superior ORR activity. To restrain the stacking interaction, which may bury active sites for ORR, between 2D heteroatom-doped graphene sheets, researchers tactfully incorporated 1D structured CNTs between graphene sheets [119–124]. The resulting CNTs/graphene hybrid exhibited good ORR activity comparable to and/or better than the commercial Pt/C catalysts under alkaline conditions. For example, Yu and coworkers, for the first time, proposed a nitrogen-doped graphene/carbon nanotube nanocomposite (NG-NCNT) as ORR catalyst. Herein, the NG-NCNT was synthesized via a hydrothermal process by using oxidized multiwalled carbon nanotube, graphene oxide, and ammonia as precursors (Figure 10a) [119]. The prepared electrode with NG-NCNT as catalyst displays much larger current and more positive onset potential than those of the NG, NCNT, G-CNT, and mixed product of GO and OCNT, respectively (Figure 10b). These indicate that the NG-NCNT possesses the best electrocatalytic ORR activity among the samples. Recently, a facile route by combining rapidly evaporating aerosol droplets with

pyrolysis process was developed to fabricate N, P co-doped CNTs/graphene hybrid nanospheres (Figure 10c,d) [125]. The obtained hybrid material shows better ORR performance than a commercial Pt/C catalyst in alkaline condition (Figure 10e). When tested in acidic solution, a comparable ORR onset potential and much better stability than the commercial Pt/C catalyst were also achieved (Figure 10f). To date, carbon nanotube/graphene hybrid structures doped with heteroatom such as N [57,122,124,126,127] and N/S [121,123] have been fabricated by different methods as promising metal-free catalysts for ORR.

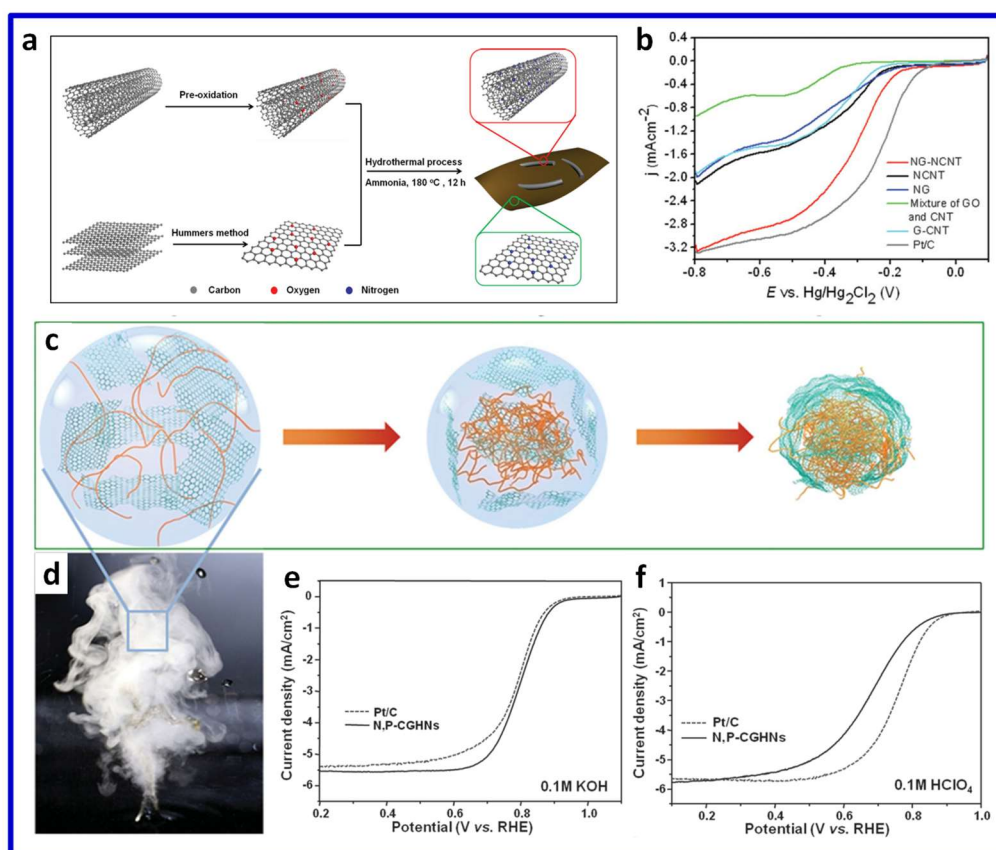


**Figure 10.** (a) Schematic illustration of the preparation of the NG-NCNT nanocomposites; (b) RDE voltammograms in  $O_2$ -saturated 0.1 M KOH solution at room temperature (rotation speed 1600 rpm, sweep rate  $20 \text{ mV} \cdot \text{s}^{-1}$ ) for the NG-NCNT, NCNT, NG, G-CNT, Pt/C and directly mixed product of GO and OCNT. Reproduced from [119], Copyright 2013, Wiley. (c) Schematic illustration of the process for co-assembling carbon nanotubes and graphene into hybrid nanospheres in rapidly evaporating aerosol droplets; (d) A photograph of the ultrasonic fountain and mist generated by a high-frequency ultrasound (1.7 MHz) from an aqueous dispersion containing oxidized carbon nanotubes and graphene oxides; (e) LSV curves of N, P-CGHNs and Pt/C in  $O_2$ -saturated 0.1 M KOH; (f) LSV curves of N, P-CGHNs and Pt/C in  $O_2$ -saturated 0.1 M  $HClO_4$ . Reproduced from [125], Copyright 2016, Wiley.

### 3.5. Other Kinds of Nanocarbon Materials for ORR

Aside from CNTs, graphene, porous carbon, and their hybrids mentioned above, other kinds of nanocarbon materials characterized with heteroatom doping and 3D structure also have been widely investigated as ORR electrocatalysts [128–131]. Nanocarbon networks especially N-doped nanocarbon networks can serve as excellent ORR catalysts. For instance, Hou et al. proposed a free-standing N-doped carbon nanotubes/carbon nanofibers hybrid (NCNT/CNFs) via simple pyrolysis of toluene or pyridine [132]. Due to the unique 3D hierarchical structure and pyridinic-N doping, the as-prepared NCNT/CNFs exhibited outstanding catalytic ORR performance with a favorable four-electron pathway, better selectivity and

resistance to the methanol crossover, and long-term stability compared to the powder-form NCNTs and commercial Pt/C catalyst in an alkaline medium. Afterwards, Yan et al. proposed a N-doped carbon nanofiber aerogel (N-CNFA) as an efficient oxygen electrode catalyst for fuel cells [133]. The optimized N-CNFA follows a favorable four-electron ORR mechanism with more stability than commercial Pt/C catalyst. This excellent performance was attributed to the hierarchical porous structure, high specific surface area, and the abundance of catalytically active sites on N-CNFA. Recently, a metal-free N- and O-doped carbon nanoweb was also developed for use as an efficient ORR catalyst for hybrid Li-air batteries [131]. The 3D web structure shows good mass and electron transport properties, which render it a better framework support for the catalytically active sites, besides, the N and O groups together create highly ORR active pyridone groups on the nanoweb surface. It is well-known that 3D flexible electrodes are the fundamental requirement of flexible energy storage and conversion systems. By simply pyrolyzing the facial cotton under  $\text{NH}_3$ , Cheng et al. prepared a 3D flexible, porous N-doped carbon microtube (NCMT) sponge as a multifunctional ORR catalyst [134]. The flexible NCMT sponge consists of a mass of interconnected fiber-like structures with a micron-scale hollow core and porous well-graphitized walls (Figure 11a,b). Owing to the synergistic advantages of micron-scale hollow cores and the intimately-interconnected, porous tube walls, the sluggish three-phase ( $\text{O}_2$ , electrolyte, and electrode) reactions efficiently proceed as illustrated in Figure 11c. The exposed surface atoms, such as C and N, provide abundant active sites. The porous walls and hollow cores within the carbon fiber promote the fast and efficient transport of  $\text{O}_2$  and electrolyte. The interconnected graphitic walls facilitate fast electron transfer. Therefore, the unique 3D structure of NCMT demonstrates excellent ORR activities with better durability than Pt/C (Figure 11d).

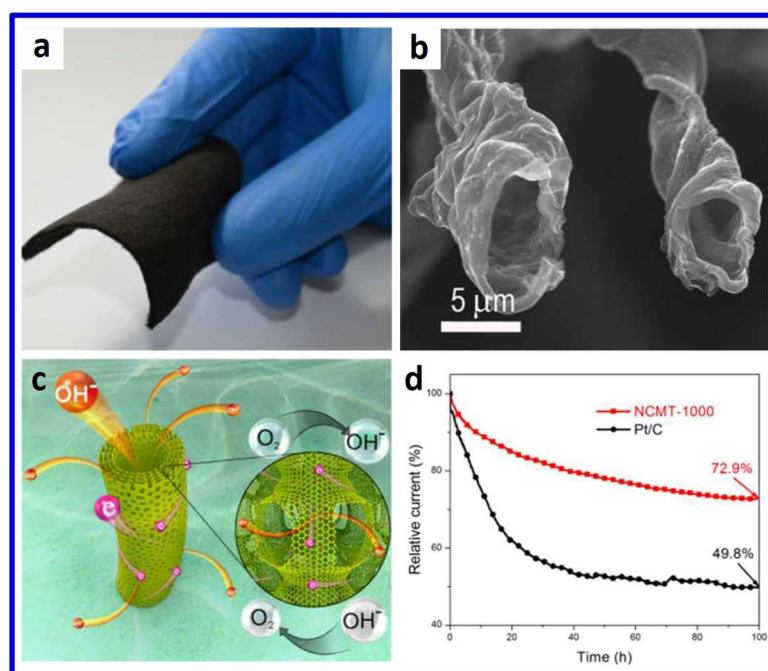


**Figure 11.** (a) Optical and (b) SEM images of NCMT-1000; (c) Schematic illustration showing the catalysis process on NCMT-1000; (d) Stability evaluation of NCMT-1000 and Pt/C tested by the chronamperometric responses. Reproduced from [134], Copyright 2016, The Royal Society of Chemistry.

More recently, N and S co-doped 3D hollow-structured carbon spheres (N,S-hcs) were synthesized via a facile and environmentally friendly route of soft template avenue as an efficient and stable metal free catalyst for the ORR [135]. Similar to the synthesis of N,S-hcs, cetyltrimethylammonium bromide (CTAB) was used as a typically pore-forming template to fabricate mesoporous 3D N-doped yolk-shelled carbon spheres (N-YS-CSs) via carbonization in the presence of carbon nitrogen precursors [136]. The mesoporous surface and particle size of N-YS-CSs can be well tuned by

controlling the amount of ammonia a catalyst, and the optimized products exhibit outstanding cathode catalytic performance for direct methanol fuel cells. Another report is that Huang's group used urchin-like hierarchical silica spheres as templates for the synthesis of uniform 3D hierarchical N-doped carbon nanoflower (NCNF) and investigated its electrocatalytic activity towards ORR [137].

#### 4. Conclusions and Perspectives

Nanocarbon-based metal-free catalysts are promising candidates originating from low cost and high-performance of ORR catalysts for fuel cells and metal–air batteries. In this review, we have summarized the recent development of advanced nanocarbon-based, metal-free ORR catalysts, including single and multiple heteroatom-doped carbon nanotubes, graphenes, and porous carbons, as well as their hybrids. The discussion of electrocatalysis has focused on the influence of 3D structure and heteroatoms on the electrochemical performance of nanocarbon catalysts. Compared with commercially available Pt/C, single nonmetal heteroatom (e.g., N, S, B, and P) or multiple heteroatom (e.g., NP, NS, NB NSO and NPO) doped nanocarbon materials show comparable or even higher electrocatalytic activity, better durability, and greater tolerance against fuel crossover and CO poisoning. The unique 3D structured nanocarbon materials can not only enhance the exposure and stability of ORR active sites, but also provide the mass transport and electron transfer pathways. Therefore, the synergetic effect between the 3D nanostructures and the doping-induced charge redistribution results in superior ORR activity.

Over the past decade, considerable progress has been made in the development of high-efficiency 3D structured nanocarbon-based ORR electrocatalysts. However, some important challenges may be addressed prior to practical applications: (1) The understanding of the activity mechanism of heteroatom-doped nanocarbon is challenging to rationally correlate the electron structure, adsorption properties, and apparent activities. For example, the nitrogen doping induces charge distribution, and parallel diatomic O<sub>2</sub> adsorption can effectively weaken the O–O bond and lower the ORR potential, facilitating oxygen reduction at the N-doped nanocarbon electrode. Some theoretical and experimental results indicate that different N doping configurations result in difference of the ORR activity and planar pyridinic N with a lone electron pair is claimed as the active type to improve the electron-donating capability and weaken the O–O bond. However, there is a debate that graphitic N rather than pyridinic N may be responsible for the ORR. Therefore, in-depth understanding of the type of active sites toward ORR and unambiguous identifying of different types of active configurations is imperative for developing advanced heteroatom-doped nanocarbon catalysts in terms of rationally selecting synthesis methods and precursors. Besides, more powerful and effective characterizations, including advanced electron microscopy and in situ or operando techniques, should be combined with theoretical calculations to identify the different active types and the actual active sites. (2) Except active sites, two other key factors of the mass transport and electrical conductivity together determine the ORR performance of a nanocarbon catalyst. Therefore, structure design and optimization of nanocarbon electrocatalysts, such as pore structure, surface area, and electrical conductivity, are significantly important to enhance their ORR performance. Generally, 3D porous structure can provide a high surface area with abundant exposed active sites and large pore volume with multidimensional electron transport pathways, and hence facilitate mass (e.g., ions, oxygen and discharge products) diffusion and electron transfer, further accelerating reaction kinetics. As discussed above, great progress has been made via designing 3D porous structures to achieve outstanding ORR performance. However, a detailed relationship between the pore structure and mass transport capability in different media is yet to be determined, and detailed models describing the transport of reactants and products within the active sites are still unclear. (3) Additionally, future efforts in the research and development of 3D nanocarbon catalysts toward ORR should focus on the tradeoffs between electrical conductivity and surface density of active sites. With continuous research in this promising field, we look forward to the bright future of 3D heteroatom-doped nanocarbon catalysts as well as the breakthroughs in the understanding of the nature of the ORR on these carbon-based metal-free ORR catalysts.

**Acknowledgments:** This work was supported by the National Natural Science Foundation of China (51572194 and 51672189), Academic Innovation Funding of Tianjin Normal University (52XC1404), Training Plan of Leader Talent of University in Tianjin, National Key R&D Program of China (2017YFB0310703), and the Fundamental Research Funds for the Central Universities (2652017369).

**Conflicts of Interest:** The authors declare no conflict of interest.

## References

1. Larcher, D.; Tarascon, J.M. Towards greener and more sustainable batteries for electrical energy storage. *Nat. Chem.* **2015**, *7*, 19–29. [[CrossRef](#)] [[PubMed](#)]
2. Qin, P.; Tanaka, S.; Ito, S.; Tetreault, N.; Manabe, K.; Nishino, H.; Nazeeruddin, M.K.; Gratzel, M. Inorganic hole conductor-based lead halide perovskite solar cells with 12.4% conversion efficiency. *Nat. Commun.* **2014**, *5*, 3834. [[CrossRef](#)] [[PubMed](#)]
3. Xiong, D.; Li, X.; Bai, Z.; Lu, S. Recent Advances in Layered  $Ti_3C_2T_x$  MXene for Electrochemical Energy Storage. *Small* **2018**, *14*, 1703419. [[CrossRef](#)] [[PubMed](#)]
4. Lu, J.; Chen, Z.; Pan, F.; Cui, Y.; Amine, K. High-Performance Anode Materials for Rechargeable Lithium-Ion Batteries. *Electrochem. Energy Rev.* **2018**, *1*, 35–53. [[CrossRef](#)]
5. Chou, S.L.; Dou, S.X. Next-Generation Batteries. *Adv. Mater.* **2017**, *29*, 1705871. [[CrossRef](#)] [[PubMed](#)]
6. Goodenough, J.B. Electrochemical energy storage in a sustainable modern society. *Energy Environ. Sci.* **2014**, *7*, 14–18. [[CrossRef](#)]
7. Cheng, F.; Chen, J. Metal-air batteries: From oxygen reduction electrochemistry to cathode catalysts. *Chem. Soc. Rev.* **2012**, *41*, 2172–2192. [[CrossRef](#)] [[PubMed](#)]
8. Li, J.C.; Hou, P.X.; Liu, C. Heteroatom-Doped Carbon Nanotube and Graphene-Based Electrocatalysts for Oxygen Reduction Reaction. *Small* **2017**, *13*, 1702002. [[CrossRef](#)] [[PubMed](#)]
9. Myles, T.; Bonville, L.; Maric, R. Catalyst, Membrane, Free Electrolyte Challenges, and Pathways to Resolutions in High Temperature Polymer Electrolyte Membrane Fuel Cells. *Catalysts* **2017**, *7*, 16. [[CrossRef](#)]
10. Suthirakun, S.; Ammal, S.C.; Munoz-Garcia, A.B.; Xiao, G.; Chen, F.; zur Loye, H.C.; Carter, E.A.; Heyden, A. Theoretical investigation of  $H_2$  oxidation on the  $Sr_2Fe_{1.5}Mo_{0.5}O_6$  (001) perovskite surface under anodic solid oxide fuel cell conditions. *J. Am. Chem. Soc.* **2014**, *136*, 8374–8386. [[CrossRef](#)] [[PubMed](#)]
11. Suntivich, J.; Gasteiger, H.A.; Yabuuchi, N.; Nakanishi, H.; Goodenough, J.B.; Shao-Horn, Y. Design principles for oxygen-reduction activity on perovskite oxide catalysts for fuel cells and metal-air batteries. *Nat. Chem.* **2011**, *3*, 546–550. [[CrossRef](#)] [[PubMed](#)]
12. Fu, S.; Zhu, C.; Song, J.; Du, D.; Lin, Y. Metal-Organic Framework-Derived Non-Precious Metal Nanocatalysts for Oxygen Reduction Reaction. *Adv. Energy Mater.* **2017**, *7*, 1700363. [[CrossRef](#)]
13. Marcel, R. Perovskite Electrocatalysts for the Oxygen Reduction Reaction in Alkaline Media. *Catalysts* **2017**, *7*, 154. [[CrossRef](#)]
14. Li, Q.; Cao, R.; Cho, J.; Wu, G. Nanocarbon Electrocatalysts for Oxygen Reduction in Alkaline Media for Advanced Energy Conversion and Storage. *Adv. Energy Mater.* **2014**, *4*, 1301415. [[CrossRef](#)]
15. Greeley, J.; Stephens, I.E.; Bondarenko, A.S.; Johansson, T.P.; Hansen, H.A.; Jaramillo, T.F.; Rossmeisl, J.; Chorkendorff, I.; Nørskov, J.K. Alloys of platinum and early transition metals as oxygen reduction electrocatalysts. *Nat. Chem.* **2009**, *1*, 552–556. [[CrossRef](#)] [[PubMed](#)]
16. Cheng, N.; Banis, M.N.; Liu, J.; Riese, A.; Li, X.; Li, R.; Ye, S.; Knights, S.; Sun, X. Extremely stable platinum nanoparticles encapsulated in a zirconia nanocage by area-selective atomic layer deposition for the oxygen reduction reaction. *Adv. Mater.* **2015**, *27*, 277–281. [[CrossRef](#)] [[PubMed](#)]
17. Guo, S.; Li, D.; Zhu, H.; Zhang, S.; Markovic, N.M.; Stamenkovic, V.R.; Sun, S. FePt and CoPt nanowires as efficient catalysts for the oxygen reduction reaction. *Angew. Chem. Int. Ed. Engl.* **2013**, *125*, 3449–3552.
18. Tan, Y.; Xu, C.; Chen, G.; Zheng, N.; Xie, Q. A graphene-platinum nanoparticles-ionic liquid composite catalyst for methanol-tolerant oxygen reduction reaction. *Energy Environ. Sci.* **2012**, *5*, 6923–6927. [[CrossRef](#)]
19. Liang, Y.; Li, Y.; Wang, H.; Zhou, J.; Wang, J.; Regier, T.; Dai, H.  $Co_3O_4$  nanocrystals on graphene as a synergistic catalyst for oxygen reduction reaction. *Nat. Mater.* **2011**, *10*, 780–786. [[CrossRef](#)] [[PubMed](#)]
20. Wang, D.; Chen, X.; Evans, D.G.; Yang, W. Well-dispersed  $Co_3O_4/Co_2MnO_4$  nanocomposites as a synergistic bifunctional catalyst for oxygen reduction and oxygen evolution reactions. *Nanoscale* **2013**, *5*, 5312–5315. [[CrossRef](#)] [[PubMed](#)]

21. Wang, Y.C.; Lai, Y.J.; Song, L.; Zhou, Z.Y.; Liu, J.G.; Wang, Q.; Yang, X.D.; Chen, C.; Shi, W.; Zheng, Y.P.; et al. S-Doping of an Fe/N/C ORR Catalyst for Polymer Electrolyte Membrane Fuel Cells with High Power Density. *Angew. Chem. Int. Ed. Engl.* **2015**, *54*, 9907–9910. [[CrossRef](#)] [[PubMed](#)]
22. Zhou, M.; Wang, H.L.; Guo, S. Towards high-efficiency nanoelectrocatalysts for oxygen reduction through engineering advanced carbon nanomaterials. *Chem. Soc. Rev.* **2016**, *45*, 1273–1307. [[CrossRef](#)] [[PubMed](#)]
23. Wang, Y.-J.; Fang, B.; Zhang, D.; Li, A.; Wilkinson, D.P.; Ignaszak, A.; Zhang, L.; Zhang, J. A Review of Carbon-Composited Materials as Air-Electrode Bifunctional Electrocatalysts for Metal–Air Batteries. *Electrochem. Energy Rev.* **2018**, *1*, 1–34. [[CrossRef](#)]
24. Liu, X.; Dai, L. Carbon-based metal-free catalysts. *Nat. Rev. Mater.* **2016**, *1*, 16064. [[CrossRef](#)]
25. Li, Q.; Zhang, S.; Dai, L.; Li, L.S. Nitrogen-doped colloidal graphene quantum dots and their size-dependent electrocatalytic activity for the oxygen reduction reaction. *J. Am. Chem. Soc.* **2012**, *134*, 18932–18935. [[CrossRef](#)] [[PubMed](#)]
26. Lin, Z.; Waller, G.; Liu, Y.; Liu, M.; Wong, C.-P. Facile Synthesis of Nitrogen-Doped Graphene via Pyrolysis of Graphene Oxide and Urea, and its Electrocatalytic Activity toward the Oxygen-Reduction Reaction. *Adv. Energy Mater.* **2012**, *2*, 884–888. [[CrossRef](#)]
27. Gong, K.; Du, F.; Xia, Z.; Durstock, M.; Dai, L. Nitrogen-doped carbon nanotube arrays with high electrocatalytic activity for oxygen reduction. *Science* **2009**, *323*, 760–764. [[CrossRef](#)] [[PubMed](#)]
28. Dai, L. Carbon-based catalysts for metal-free electrocatalysis. *Curr. Opin. Electrochem.* **2017**, *4*, 18–25. [[CrossRef](#)]
29. Zheng, Y.; Jiao, Y.; Jaroniec, M.; Jin, Y.; Qiao, S.Z. Nanostructured metal-free electrochemical catalysts for highly efficient oxygen reduction. *Small* **2012**, *8*, 3550–3566. [[CrossRef](#)] [[PubMed](#)]
30. Zhu, Y.P.; Guo, C.; Zheng, Y.; Qiao, S.Z. Surface and Interface Engineering of Noble-Metal-Free Electrocatalysts for Efficient Energy Conversion Processes. *Acc. Chem. Res.* **2017**, *50*, 915–923. [[CrossRef](#)] [[PubMed](#)]
31. Zhang, J.; Dai, L. Heteroatom-Doped Graphitic Carbon Catalysts for Efficient Electrocatalysis of Oxygen Reduction Reaction. *ACS Catal.* **2015**, *5*, 7244–7253. [[CrossRef](#)]
32. Tang, C.; Zhang, Q. Nanocarbon for Oxygen Reduction Electrocatalysis: Dopants, Edges, and Defects. *Adv. Mater.* **2017**, *29*, 1604103. [[CrossRef](#)] [[PubMed](#)]
33. He, W.; Wang, Y.; Jiang, C.; Lu, L. Structural effects of a carbon matrix in non-precious metal O<sub>2</sub>-reduction electrocatalysts. *Chem. Soc. Rev.* **2016**, *45*, 2396–2409. [[CrossRef](#)] [[PubMed](#)]
34. Tu, Y.; Deng, D.; Bao, X. Nanocarbons and their hybrids as catalysts for non-aqueous lithium–oxygen batteries. *J. Energy Chem.* **2016**, *25*, 957–966. [[CrossRef](#)]
35. Sawant, S.Y.; Han, T.H.; Cho, M.H. Metal-Free Carbon-Based Materials: Promising Electrocatalysts for Oxygen Reduction Reaction in Microbial Fuel Cells. *Int. J. Mol. Sci.* **2016**, *18*, 25. [[CrossRef](#)] [[PubMed](#)]
36. Higgins, D.; Zamani, P.; Yu, A.; Chen, Z. The application of graphene and its composites in oxygen reduction electrocatalysis: A perspective and review of recent progress. *Energy Environ. Sci.* **2016**, *9*, 357–390. [[CrossRef](#)]
37. Du, R.; Zhang, N.; Zhu, J.; Wang, Y.; Xu, C.; Hu, Y.; Mao, N.; Xu, H.; Duan, W.; Zhuang, L.; et al. Nitrogen-Doped Carbon Nanotube Aerogels for High-Performance ORR Catalysts. *Small* **2015**, *11*, 3903–3908. [[CrossRef](#)] [[PubMed](#)]
38. Tang, S.; Zhou, X.; Xu, N.; Bai, Z.; Qiao, J.; Zhang, J. Template-free synthesis of three-dimensional nanoporous N-doped graphene for high performance fuel cell oxygen reduction reaction in alkaline media. *Appl. Energy* **2016**, *175*, 405–413. [[CrossRef](#)]
39. Jiang, H.; Zhu, Y.; Feng, Q.; Su, Y.; Yang, X.; Li, C. Nitrogen and phosphorus dual-doped hierarchical porous carbon foams as efficient metal-free electrocatalysts for oxygen reduction reactions. *Chem. Eur. J.* **2014**, *20*, 3106–3112. [[CrossRef](#)] [[PubMed](#)]
40. Yang, Z.; Nie, H.; Chen, X.A.; Chen, X.; Huang, S. Recent progress in doped carbon nanomaterials as effective cathode catalysts for fuel cell oxygen reduction reaction. *J. Power Sources* **2013**, *236*, 238–249. [[CrossRef](#)]
41. Liu, J.; Song, P.; Ning, Z.; Xu, W. Recent Advances in Heteroatom-Doped Metal-Free Electrocatalysts for Highly Efficient Oxygen Reduction Reaction. *Electrocatalysis* **2015**, *6*, 132–147. [[CrossRef](#)]
42. Ma, R.; Ma, Y.; Dong, Y.; Lee, J.-M. Recent Advances in Heteroatom-Doped Graphene Materials as Efficient Electrocatalysts towards the Oxygen Reduction Reaction. *Nano Adv.* **2016**, *1*, 50–61. [[CrossRef](#)]
43. Zhang, L.; Xia, Z. Mechanisms of Oxygen Reduction Reaction on Nitrogen-Doped Graphene for Fuel Cells. *J. Phys. Chem. C* **2011**, *115*, 11170–11176. [[CrossRef](#)]

44. Carrette, L.; Friedrich, K.A.; Stimming, U. Fuel Cells—Fundamentals and Applications. *Fuel Cells* **2001**, *1*, 5–39. [[CrossRef](#)]
45. Liew, K.B.; Daud, W.R.W.; Ghasemi, M.; Leong, J.X.; Lim, S.S.; Ismail, M. Non-Pt catalyst as oxygen reduction reaction in microbial fuel cells: A review. *Int. J. Hydrog. Energy* **2014**, *39*, 4870–4883. [[CrossRef](#)]
46. Gu, W.; Hu, L.; Li, J.; Wang, E. Recent Advancements in Transition Metal-Nitrogen-Carbon Catalysts for Oxygen Reduction Reaction. *Electroanalysis* **2018**. [[CrossRef](#)]
47. Stacy, J.; Regmi, Y.N.; Leonard, B.; Fan, M. The recent progress and future of oxygen reduction reaction catalysis: A review. *Renew. Sustain. Energy Rev.* **2017**, *69*, 401–414. [[CrossRef](#)]
48. Shui, J.; Wang, M.; Du, F.; Dai, L. N-doped carbon nanomaterials are durable catalysts for oxygen reduction reaction in acidic fuel cells. *Sci. Adv.* **2015**, *1*, 1400129. [[CrossRef](#)] [[PubMed](#)]
49. Xiong, D.; Li, X.; Shan, H.; Yan, B.; Dong, L.; Cao, Y.; Li, D. Controllable oxygenic functional groups of metal-free cathodes for high performance lithium ion batteries. *J. Mater. Chem. A* **2015**, *3*, 11376–11386. [[CrossRef](#)]
50. Xiong, D.; Li, X.; Shan, H.; Yan, B.; Li, D.; Langford, C.; Sun, X. Scalable synthesis of functionalized graphene as cathodes in Li-ion electrochemical energy storage devices. *Appl. Energy* **2016**, *175*, 512–521. [[CrossRef](#)]
51. Li, C.; Zhang, X.; Wang, K.; Zhang, H.-T.; Sun, X.-Z.; Ma, Y.-W. Three dimensional graphene networks for supercapacitor electrode materials. *New Carbon Mater.* **2015**, *30*, 193–206. [[CrossRef](#)]
52. Lin, Z.; Zeng, Z.; Gui, X.; Tang, Z.; Zou, M.; Cao, A. Carbon Nanotube Sponges, Aerogels, and Hierarchical Composites: Synthesis, Properties, and Energy Applications. *Adv. Energy Mater.* **2016**, *6*, 1600554. [[CrossRef](#)]
53. Tang, J.; Liu, J.; Torad, N.L.; Kimura, T.; Yamauchi, Y. Tailored design of functional nanoporous carbon materials toward fuel cell applications. *Nano Today* **2014**, *9*, 305–323. [[CrossRef](#)]
54. Daems, N.; Sheng, X.; Vankelecom, F.J.; Pescarmona, P.P. Metal-free doped carbon materials as electrocatalysts for the oxygen reduction reaction. *J. Mater. Chem. A* **2014**, *2*, 4085–4110. [[CrossRef](#)]
55. Ito, Y.; Qiu, H.J.; Fujita, T.; Tanabe, Y.; Tanigaki, K.; Chen, M. Bicontinuous nanoporous N-doped graphene for the oxygen reduction reaction. *Adv. Mater.* **2014**, *26*, 4145–4150. [[CrossRef](#)] [[PubMed](#)]
56. Wang, Y.; Tao, L.; Xiao, Z.; Chen, R.; Jiang, Z.; Wang, S. 3D Carbon Electrocatalysts In Situ Constructed by Defect-Rich Nanosheets and Polyhedrons from NaCl-Sealed Zeolitic Imidazolate Frameworks. *Adv. Funct. Mater.* **2018**, *28*, 1705356. [[CrossRef](#)]
57. Tian, G.L.; Zhao, M.Q.; Yu, D.; Kong, X.Y.; Huang, J.Q.; Zhang, Q.; Wei, F. Nitrogen-doped graphene/carbon nanotube hybrids: In situ formation on bifunctional catalysts and their superior electrocatalytic activity for oxygen evolution/reduction reaction. *Small* **2014**, *10*, 2251–2259. [[CrossRef](#)] [[PubMed](#)]
58. Avouris, P.; Dimitrakopoulos, C. Graphene: Synthesis and applications. *Mater. Today* **2012**, *15*, 86–97. [[CrossRef](#)]
59. Xiao, X.; Peng, X.; Jin, H.; Li, T.; Zhang, C.; Gao, B.; Hu, B.; Huo, K.; Zhou, J. Freestanding mesoporous VN/CNT hybrid electrodes for flexible all-solid-state supercapacitors. *Adv. Mater.* **2013**, *25*, 5091–5097. [[CrossRef](#)] [[PubMed](#)]
60. Yang, L.; Jiang, S.; Zhao, Y.; Zhu, L.; Chen, S.; Wang, X.; Wu, Q.; Ma, J.; Ma, Y.; Hu, Z. Boron-doped carbon nanotubes as metal-free electrocatalysts for the oxygen reduction reaction. *Angew. Chem. Int. Ed. Engl.* **2011**, *50*, 7132–7135. [[CrossRef](#)] [[PubMed](#)]
61. Yu, D.; Xue, Y.; Dai, L. Vertically Aligned Carbon Nanotube Arrays Co-doped with Phosphorus and Nitrogen as Efficient Metal-Free Electrocatalysts for Oxygen Reduction. *J. Phys. Chem. Lett.* **2012**, *3*, 2863–2870. [[CrossRef](#)] [[PubMed](#)]
62. Yu, D.; Zhang, Q.; Dai, L. Highly efficient metal-free growth of nitrogen-doped single-walled carbon nanotubes on plasma-etched substrates for oxygen reduction. *J. Am. Chem. Soc.* **2010**, *132*, 15127–15129. [[CrossRef](#)] [[PubMed](#)]
63. Wang, Z.; Jia, R.; Zheng, J.; Zhao, J.; Li, L.; Song, J.; Zhu, Z. Nitrogen-promoted self-assembly of N-doped carbon nanotubes and their intrinsic catalysis for oxygen reduction in fuel cells. *ACS Nano* **2011**, *5*, 1677–1684. [[CrossRef](#)] [[PubMed](#)]
64. Pan, T.; Liu, H.; Ren, G.; Li, Y.; Lu, X.; Zhu, Y. Metal-free porous nitrogen-doped carbon nanotubes for enhanced oxygen reduction and evolution reactions. *Sci. Bull.* **2016**, *61*, 889–896. [[CrossRef](#)]
65. She, X.; Yang, D.; Jing, D.; Yuan, F.; Yang, W.; Guo, L.; Che, Y. Nitrogen-doped one-dimensional (1D) macroporous carbonaceous nanotube arrays and their application in electrocatalytic oxygen reduction reactions. *Nanoscale* **2014**, *6*, 11057–11061. [[CrossRef](#)] [[PubMed](#)]

66. Xiong, W.; Du, F.; Liu, Y.; Perez, A., Jr.; Supp, M.; Ramakrishnan, T.S.; Dai, L.; Jiang, L. 3-D carbon nanotube structures used as high performance catalyst for oxygen reduction reaction. *J. Am. Chem. Soc.* **2010**, *132*, 15839–15841. [[CrossRef](#)] [[PubMed](#)]
67. Qi, J.; Benipal, N.; Chadderton, D.J.; Huo, J.; Jiang, Y.; Qiu, Y.; Han, X.; Hu, Y.H.; Shanks, B.H.; Li, W. Carbon nanotubes as catalysts for direct carbohydrazide fuel cells. *Carbon* **2015**, *89*, 142–147. [[CrossRef](#)]
68. Guo, M.-Q.; Huang, J.-Q.; Kong, X.-Y.; Peng, H.-J.; Shui, H.; Qian, F.-Y.; Zhu, L.; Zhu, W.-C.; Zhang, Q. Hydrothermal synthesis of porous phosphorus-doped carbon nanotubes and their use in the oxygen reduction reaction and lithium-sulfur batteries. *New Carbon Mater.* **2016**, *31*, 352–362. [[CrossRef](#)]
69. Liu, Z.; Peng, F.; Wang, H.; Yu, H.; Tan, J.; Zhu, L. Novel phosphorus-doped multiwalled nanotubes with high electrocatalytic activity for O<sub>2</sub> reduction in alkaline medium. *Catal. Commun.* **2011**, *16*, 35–38. [[CrossRef](#)]
70. Zhu, J.; Jiang, S.P.; Wang, R.; Shi, K.; Shen, P.K. One-pot synthesis of a nitrogen and phosphorus-dual-doped carbon nanotube array as a highly effective electrocatalyst for the oxygen reduction reaction. *J. Mater. Chem. A* **2014**, *2*, 15448–15453. [[CrossRef](#)]
71. Bonaccorso, F.; Colombo, L.; Yu, G.; Stoller, M.; Tozzini, V.; Ferrari, A.C.; Ruoff, R.S.; Pellegrini, V. 2D materials. Graphene, related two-dimensional crystals, and hybrid systems for energy conversion and storage. *Science* **2015**, *347*, 1246501. [[CrossRef](#)] [[PubMed](#)]
72. Cao, X.; Yin, Z.; Zhang, H. Three-dimensional graphene materials: Preparation, structures and application in supercapacitors. *Energy Environ. Sci.* **2014**, *7*, 1850–1865. [[CrossRef](#)]
73. Hu, C.; Liu, D.; Xiao, Y.; Dai, L. Functionalization of graphene materials by heteroatom-doping for energy conversion and storage. *Prog. Nat. Sci. Mater.* **2018**. [[CrossRef](#)]
74. Xiong, D.; Li, X.; Bai, Z.; Shan, H.; Fan, L.; Wu, C.; Li, D.; Lu, S. Superior Cathode Performance of Nitrogen-Doped Graphene Frameworks for Lithium Ion Batteries. *ACS Appl. Mater. Interfaces* **2017**, *9*, 10643–10651. [[CrossRef](#)] [[PubMed](#)]
75. Shan, H.; Li, X.; Cui, Y.; Xiong, D.; Yan, B.; Li, D.; Lushington, A.; Sun, X. Sulfur/Nitrogen Dual-doped Porous Graphene Aerogels Enhancing Anode Performance of Lithium Ion Batteries. *Electrochim. Acta* **2016**, *205*, 188–197. [[CrossRef](#)]
76. Sheng, Z.H.; Shao, L.; Chen, J.J.; Bao, W.J.; Wang, F.B.; Xia, X.H. Catalyst-free synthesis of nitrogen-doped graphene via thermal annealing graphite oxide with melamine and its excellent electrocatalysis. *ACS Nano* **2011**, *5*, 4350–4358. [[CrossRef](#)] [[PubMed](#)]
77. Yang, Z.; Yao, Z.; Li, G.; Fang, G.; Nie, H.; Liu, Z.; Zhou, X.; Chen, X.; Huang, S. Sulfur-doped graphene as an efficient metal-free cathode catalyst for oxygen reduction. *ACS Nano* **2011**, *6*, 205–211. [[CrossRef](#)] [[PubMed](#)]
78. Jo, G.; Sanetuntikul, J.; Shanmugam, S. Boron and phosphorous-doped graphene as a metal-free electrocatalyst for the oxygen reduction reaction in alkaline medium. *RSC Adv.* **2015**, *5*, 53637–53643. [[CrossRef](#)]
79. Su, Y.; Zhang, Y.; Zhuang, X.; Li, S.; Wu, D.; Zhang, F.; Feng, X. Low-temperature synthesis of nitrogen/sulfur co-doped three-dimensional graphene frameworks as efficient metal-free electrocatalyst for oxygen reduction reaction. *Carbon* **2013**, *62*, 296–301. [[CrossRef](#)]
80. Xue, Y.; Yu, D.; Dai, L.; Wang, R.; Li, D.; Roy, A.; Lu, F.; Chen, H.; Liu, Y.; Qu, J. Three-dimensional B,N-doped graphene foam as a metal-free catalyst for oxygen reduction reaction. *Phys. Chem. Chem. Phys.* **2013**, *15*, 12220–12226. [[CrossRef](#)] [[PubMed](#)]
81. Chen, L.; Du, R.; Zhu, J.; Mao, Y.; Xue, C.; Zhang, N.; Hou, Y.; Zhang, J.; Yi, T. Three-dimensional nitrogen-doped graphene nanoribbons aerogel as a highly efficient catalyst for the oxygen reduction reaction. *Small* **2015**, *11*, 1423–1429. [[CrossRef](#)] [[PubMed](#)]
82. Guan, Y.; Dou, Z.; Yang, Y.; Xue, J.; Zhu, Z.; Cui, L. Fabrication of functionalized 3D graphene with controllable micro/meso-pores as a superior electrocatalyst for enhanced oxygen reduction in both acidic and alkaline solutions. *RSC Adv.* **2016**, *6*, 79459–79469. [[CrossRef](#)]
83. Qu, L.; Liu, Y.; Baek, J.B.; Dai, L. Nitrogen-doped graphene as efficient metal-free electrocatalyst for oxygen reduction in fuel cells. *ACS Nano* **2010**, *4*, 1321–1326. [[CrossRef](#)] [[PubMed](#)]
84. Shan, H.; Xiong, D.; Li, X.; Sun, Y.; Yan, B.; Li, D.; Lawes, S.; Cui, Y.; Sun, X. Tailored lithium storage performance of graphene aerogel anodes with controlled surface defects for lithium-ion batteries. *Appl. Surf. Sci.* **2016**, *364*, 651–659. [[CrossRef](#)]

85. Kabir, S.; Artyushkova, K.; Serov, A.; Atanassov, P. Role of Nitrogen Moieties in N-Doped 3D-Graphene Nanosheets for Oxygen Electroreduction in Acidic and Alkaline Media. *ACS Appl. Mater. Interfaces* **2018**, *10*, 11623–11632. [[CrossRef](#)] [[PubMed](#)]
86. Zhao, C.; Yu, C.; Liu, S.; Yang, J.; Fan, X.; Huang, H.; Qiu, J. 3D Porous N-Doped Graphene Frameworks Made of Interconnected Nanocages for Ultrahigh-Rate and Long-Life Li–O<sub>2</sub> Batteries. *Adv. Funct. Mater.* **2015**, *25*, 6913–6920. [[CrossRef](#)]
87. Shi, J.-L.; Tang, C.; Huang, J.-Q.; Zhu, W.; Zhang, Q. Effective exposure of nitrogen heteroatoms in 3D porous graphene framework for oxygen reduction reaction and lithium–sulfur batteries. *J. Energy Chem.* **2018**, *27*, 167–175. [[CrossRef](#)]
88. Lu, X.; Li, Z.; Yin, X.; Wang, S.; Liu, Y.; Wang, Y. Controllable synthesis of three-dimensional nitrogen-doped graphene as a high performance electrocatalyst for oxygen reduction reaction. *Int. J. Hydrog. Energy* **2017**, *42*, 17504–17513. [[CrossRef](#)]
89. Chen, X.; Chen, X.; Xu, X.; Yang, Z.; Liu, Z.; Zhang, L.; Xu, X.; Chen, Y.; Huang, S. Sulfur-doped porous reduced graphene oxide hollow nanosphere frameworks as metal-free electrocatalysts for oxygen reduction reaction and as supercapacitor electrode materials. *Nanoscale* **2014**, *6*, 13740–13747. [[CrossRef](#)] [[PubMed](#)]
90. Zhang, Y.; Chu, M.; Yang, L.; Deng, W.; Tan, Y.; Ma, M.; Xie, Q. Synthesis and oxygen reduction properties of three-dimensional sulfur-doped graphene networks. *Chem. Commun.* **2014**, *50*, 6382–6385. [[CrossRef](#)] [[PubMed](#)]
91. Li, X.; Qiu, Y.; Hu, P.A. Three Dimensional P-doped Graphene Synthesized by Eco-Friendly Chemical Vapor Deposition for Oxygen Reduction Reactions. *J. Nanosci. Nanotechnol.* **2016**, *16*, 6216–6222. [[CrossRef](#)] [[PubMed](#)]
92. Liang, J.; Jiao, Y.; Jaroniec, M.; Qiao, S.Z. Sulfur and nitrogen dual-doped mesoporous graphene electrocatalyst for oxygen reduction with synergistically enhanced performance. *Angew. Chem. Int. Ed. Engl.* **2012**, *51*, 11496–11500. [[CrossRef](#)] [[PubMed](#)]
93. Xu, C.; Su, Y.; Liu, D.; He, X. Three-dimensional N,B-doped graphene aerogel as a synergistically enhanced metal-free catalyst for the oxygen reduction reaction. *Phys. Chem. Chem. Phys.* **2015**, *17*, 25440–25448. [[CrossRef](#)] [[PubMed](#)]
94. Amiin, I.S.; Zhang, J.; Kou, Z.; Liu, X.; Asare, O.K.; Zhou, H.; Cheng, K.; Zhang, H.; Mai, L.; Pan, M.; et al. Self-Organized 3D Porous Graphene Dual-Doped with Biomass-Sponsored Nitrogen and Sulfur for Oxygen Reduction and Evolution. *ACS Appl. Mater. Interfaces* **2016**, *8*, 29408–29418. [[CrossRef](#)] [[PubMed](#)]
95. Rivera, L.M.; Fajardo, S.; Arévalo, M.D.C.; García, G.; Pastor, E. S- and N-Doped Graphene Nanomaterials for the Oxygen Reduction Reaction. *Catalysts* **2017**, *7*, 278. [[CrossRef](#)]
96. Chabu, J.M.; Wang, L.; Tang, F.-Y.; Zeng, K.; Sheng, J.; Walle, M.D.; Deng, L.; Liu, Y.-N. Synthesis of Three-Dimensional Nitrogen and Sulfur Dual-Doped Graphene Aerogels as an Efficient Metal-Free Electrocatalyst for the Oxygen Reduction Reaction. *ChemElectroChem* **2017**, *4*, 1885–1890. [[CrossRef](#)]
97. Wu, M.; Dou, Z.; Chang, J.; Cui, L. Nitrogen and sulfur co-doped graphene aerogels as an efficient metal-free catalyst for oxygen reduction reaction in an alkaline solution. *RSC Adv.* **2016**, *6*, 22781–22790. [[CrossRef](#)]
98. Li, Y.; Yang, J.; Huang, J.; Zhou, Y.; Xu, K.; Zhao, N.; Cheng, X. Soft template-assisted method for synthesis of nitrogen and sulfur co-doped three-dimensional reduced graphene oxide as an efficient metal free catalyst for oxygen reduction reaction. *Carbon* **2017**, *122*, 237–246. [[CrossRef](#)]
99. Zhao, Y.; Huang, S.; Xia, M.; Rehman, S.; Mu, S.; Kou, Z.; Zhang, Z.; Chen, Z.; Gao, F.; Hou, Y. N-P-O co-doped high performance 3D graphene prepared through red phosphorous-assisted “cutting-thin” technique: A universal synthesis and multifunctional applications. *Nano Energy* **2016**, *28*, 346–355. [[CrossRef](#)]
100. Liu, R.; Wu, D.; Feng, X.; Mullen, K. Nitrogen-doped ordered mesoporous graphitic arrays with high electrocatalytic activity for oxygen reduction. *Angew. Chem. Int. Ed. Engl.* **2010**, *49*, 2565–2569. [[CrossRef](#)] [[PubMed](#)]
101. Liu, Z.; Nie, H.; Yang, Z.; Zhang, J.; Jin, Z.; Lu, Y.; Xiao, Z.; Huang, S. Sulfur-nitrogen co-doped three-dimensional carbon foams with hierarchical pore structures as efficient metal-free electrocatalysts for oxygen reduction reactions. *Nanoscale* **2013**, *5*, 3283–3288. [[CrossRef](#)] [[PubMed](#)]
102. Liang, H.W.; Zhuang, X.; Bruller, S.; Feng, X.; Mullen, K. Hierarchically porous carbons with optimized nitrogen doping as highly active electrocatalysts for oxygen reduction. *Nat. Commun.* **2014**, *5*, 4973. [[CrossRef](#)] [[PubMed](#)]

103. Chen, Y.; Ma, R.; Zhou, Z.; Liu, G.; Zhou, Y.; Liu, Q.; Kaskel, S.; Wang, J. An In Situ Source-Template-Interface Reaction Route to 3D Nitrogen-Doped Hierarchical Porous Carbon as Oxygen Reduction Electrocatalyst. *Adv. Mater. Interfaces* **2015**, *2*, 1500199. [[CrossRef](#)]
104. Zhu, C.; Li, H.; Fu, S.; Du, D.; Lin, Y. Highly efficient nonprecious metal catalysts towards oxygen reduction reaction based on three-dimensional porous carbon nanostructures. *Chem. Soc. Rev.* **2016**, *45*, 517–531. [[CrossRef](#)] [[PubMed](#)]
105. Chen, S.; Bi, J.; Zhao, Y.; Yang, L.; Zhang, C.; Ma, Y.; Wu, Q.; Wang, X.; Hu, Z. Nitrogen-doped carbon nanocages as efficient metal-free electrocatalysts for oxygen reduction reaction. *Adv. Mater.* **2012**, *24*, 5593–5597. [[CrossRef](#)] [[PubMed](#)]
106. Gao, S.; Chen, Y.; Fan, H.; Wei, X.; Hu, C.; Luo, H.; Qu, L. Large scale production of biomass-derived N-doped porous carbon spheres for oxygen reduction and supercapacitors. *J. Mater. Chem. A* **2014**, *2*, 3317–3324. [[CrossRef](#)]
107. Huang, H.; Wei, X.; Gao, S. Nitrogen-Doped Porous Carbon Derived from Malachium Aquaticum Biomass as a Highly Efficient Electrocatalyst for Oxygen Reduction Reaction. *Electrochim. Acta* **2016**, *220*, 427–435. [[CrossRef](#)]
108. Liu, R.; Zhang, H.; Liu, S.; Zhang, X.; Wu, T.; Ge, X.; Zang, Y.; Zhao, H.; Wang, G. Shrimp-shell derived carbon nanodots as carbon and nitrogen sources to fabricate three-dimensional N-doped porous carbon electrocatalysts for the oxygen reduction reaction. *Phys. Chem. Chem. Phys.* **2016**, *18*, 4095–4101. [[CrossRef](#)] [[PubMed](#)]
109. Zhang, J.; Zhang, C.; Zhao, Y.; Amiin, I.S.; Zhou, H.; Liu, X.; Tang, Y.; Mu, S. Three dimensional few-layer porous carbon nanosheets towards oxygen reduction. *Appl. Catal. B-Environ.* **2017**, *211*, 148–156. [[CrossRef](#)]
110. Zhong, H.X.; Wang, J.; Zhang, Y.W.; Xu, W.L.; Xing, W.; Xu, D.; Zhang, Y.F.; Zhang, X.B. ZIF-8 derived graphene-based nitrogen-doped porous carbon sheets as highly efficient and durable oxygen reduction electrocatalysts. *Angew. Chem. Int. Ed. Engl.* **2014**, *53*, 14235–14239. [[CrossRef](#)] [[PubMed](#)]
111. Yu, H.; Shang, L.; Bian, T.; Shi, R.; Waterhouse, G.I.; Zhao, Y.; Zhou, C.; Wu, L.Z.; Tung, C.H.; Zhang, T. Nitrogen-Doped Porous Carbon Nanosheets Templated from g-C<sub>3</sub>N<sub>4</sub> as Metal-Free Electrocatalysts for Efficient Oxygen Reduction Reaction. *Adv. Mater.* **2016**, *28*, 5080–5086. [[CrossRef](#)] [[PubMed](#)]
112. Chen, C.; Sun, Z.; Li, Y.; Yi, L.; Hu, H. Self-assembly of N doped 3D porous carbon frameworks from carbon quantum dots and its application for oxygen reduction reaction. *J. Mater. Sci.-Mater. Electron.* **2017**, *28*, 12660–12669. [[CrossRef](#)]
113. Li, X.; Xue, X.; Fu, Y. Carbon Quantum Dots Derived N-Doped Porous Carbon Frameworks with High Electrocatalytic for Oxygen Reduction Reaction. *Nano* **2017**, *12*, 1750093. [[CrossRef](#)]
114. Luo, E.; Xiao, M.; Ge, J.; Liu, C.; Xing, W. Selectively doping pyridinic and pyrrolic nitrogen into a 3D porous carbon matrix through template-induced edge engineering: Enhanced catalytic activity towards the oxygen reduction reaction. *J. Mater. Chem. A* **2017**, *5*, 21709–21714. [[CrossRef](#)]
115. Wang, Y.; Liu, H.; Wang, K.; Song, S.; Tsiakaras, P. 3D interconnected hierarchically porous N-doped carbon with NH<sub>3</sub> activation for efficient oxygen reduction reaction. *Appl. Catal. B-Environ.* **2017**, *210*, 57–66. [[CrossRef](#)]
116. Huang, X.; Wang, Q.; Jiang, D.; Huang, Y. Facile synthesis of B, N co-doped three-dimensional porous graphitic carbon toward oxygen reduction reaction and oxygen evolution reaction. *Catal. Commun.* **2017**, *100*, 89–92. [[CrossRef](#)]
117. Jiang, H.; Wang, Y.; Hao, J.; Liu, Y.; Li, W.; Li, J. N and P co-functionalized three-dimensional porous carbon networks as efficient metal-free electrocatalysts for oxygen reduction reaction. *Carbon* **2017**, *122*, 64–73. [[CrossRef](#)]
118. Pei, Z.; Li, H.; Huang, Y.; Xue, Q.; Huang, Y.; Zhu, M.; Wang, Z.; Zhi, C. Texturing in situ: N,S-enriched hierarchically porous carbon as a highly active reversible oxygen electrocatalyst. *Energy Environ. Sci.* **2017**, *10*, 742–749. [[CrossRef](#)]
119. Chen, P.; Xiao, T.Y.; Qian, Y.H.; Li, S.S.; Yu, S.H. A nitrogen-doped graphene/carbon nanotube nanocomposite with synergistically enhanced electrochemical activity. *Adv. Mater.* **2013**, *25*, 3192–3196. [[CrossRef](#)] [[PubMed](#)]
120. Lee, J.-S.; Jo, K.; Lee, T.; Yun, T.; Cho, J.; Kim, B.-S. Facile synthesis of hybrid graphene and carbon nanotubes as a metal-free electrocatalyst with active dual interfaces for efficient oxygen reduction reaction. *J. Mater. Chem. A* **2013**, *1*, 9603–9607. [[CrossRef](#)]
121. Higgins, D.C.; Hoque, M.A.; Hassan, F.; Choi, J.-Y.; Kim, B.; Chen, Z. Oxygen Reduction on Graphene–Carbon Nanotube Composites Doped Sequentially with Nitrogen and Sulfur. *ACS Catal.* **2014**, *4*, 2734–2740. [[CrossRef](#)]

122. Liu, J.Y.; Wang, Z.; Chen, J.Y.; Wang, X. Nitrogen-Doped Carbon Nanotubes and Graphene Nanohybrid for Oxygen Reduction Reaction in Acidic, Alkaline and Neutral Solutions. *J. Nano Res.* **2015**, *30*, 50–58. [[CrossRef](#)]
123. Zhao, J.; Liu, Y.; Quan, X.; Chen, S.; Zhao, H.; Yu, H. Nitrogen and sulfur co-doped graphene/carbon nanotube as metal-free electrocatalyst for oxygen evolution reaction: The enhanced performance by sulfur doping. *Electrochim. Acta* **2016**, *204*, 169–175. [[CrossRef](#)]
124. Ma, Y.; Sun, L.; Huang, W.; Zhang, L.; Zhao, J.; Fan, Q.; Huang, W. Three-Dimensional Nitrogen-Doped Carbon Nanotubes/Graphene Structure Used as a Metal-Free Electrocatalyst for the Oxygen Reduction Reaction. *J. Phys. Chem. C* **2011**, *115*, 24592–24597. [[CrossRef](#)]
125. Yang, J.; Sun, H.; Liang, H.; Ji, H.; Song, L.; Gao, C.; Xu, H. A Highly Efficient Metal-Free Oxygen Reduction Electrocatalyst Assembled from Carbon Nanotubes and Graphene. *Adv. Mater.* **2016**, *28*, 4606–4613. [[CrossRef](#)] [[PubMed](#)]
126. Shi, Q.; Wang, Y.; Wang, Z.; Lei, Y.; Wang, B.; Wu, N.; Han, C.; Xie, S.; Gou, Y. Three-dimensional (3D) interconnected networks fabricated via in-situ growth of N-doped graphene/carbon nanotubes on Co-containing carbon nanofibers for enhanced oxygen reduction. *Nano Res.* **2015**, *9*, 317–328. [[CrossRef](#)]
127. Li, Y.; Zhou, W.; Wang, H.; Xie, L.; Liang, Y.; Wei, F.; Idrobo, J.C.; Pennycook, S.J.; Dai, H. An oxygen reduction electrocatalyst based on carbon nanotube-graphene complexes. *Nat. Nanotechnol.* **2012**, *7*, 394–400. [[CrossRef](#)] [[PubMed](#)]
128. Zhang, J.; Qu, L.; Shi, G.; Liu, J.; Chen, J.; Dai, L. N,P-Codoped Carbon Networks as Efficient Metal-free Bifunctional Catalysts for Oxygen Reduction and Hydrogen Evolution Reactions. *Angew. Chem. Int. Ed. Engl.* **2016**, *55*, 2230–2234. [[CrossRef](#)] [[PubMed](#)]
129. Chen, Y.; Wang, H.; Ji, S.; Lv, W.; Wang, R. Harvesting a 3D N-Doped Carbon Network from Waste Bean Dregs by Ionothermal Carbonization as an Electrocatalyst for an Oxygen Reduction Reaction. *Materials* **2017**, *10*, 1366. [[CrossRef](#)] [[PubMed](#)]
130. Mulyadi, A.; Zhang, Z.; Dutzer, M.; Liu, W.; Deng, Y. Facile approach for synthesis of doped carbon electrocatalyst from cellulose nanofibrils toward high-performance metal-free oxygen reduction and hydrogen evolution. *Nano Energy* **2017**, *32*, 336–346. [[CrossRef](#)]
131. Li, L.; Manthiram, A. O- and N-Doped Carbon Nanowebs as Metal-Free Catalysts for Hybrid Li-Air Batteries. *Adv. Energy Mater.* **2014**, *4*, 1301795. [[CrossRef](#)]
132. Guo, Q.; Zhao, D.; Liu, S.; Chen, S.; Hanif, M.; Hou, H. Free-standing nitrogen-doped carbon nanotubes at electrospun carbon nanofibers composite as an efficient electrocatalyst for oxygen reduction. *Electrochim. Acta* **2014**, *138*, 318–324. [[CrossRef](#)]
133. Meng, F.; Li, L.; Wu, Z.; Zhong, H.; Li, J.; Yan, J. Facile preparation of N-doped carbon nanofiber aerogels from bacterial cellulose as an efficient oxygen reduction reaction electrocatalyst. *Chin. J. Catal.* **2014**, *35*, 877–883. [[CrossRef](#)]
134. Li, J.-C.; Hou, P.-X.; Zhao, S.-Y.; Liu, C.; Tang, D.-M.; Cheng, M.; Zhang, F.; Cheng, H.-M. A 3D bi-functional porous N-doped carbon microtube sponge electrocatalyst for oxygen reduction and oxygen evolution reactions. *Energy Environ. Sci.* **2016**, *9*, 3079–3084. [[CrossRef](#)]
135. Wu, Z.; Liu, R.; Wang, J.; Zhu, J.; Xiao, W.; Xuan, C.; Lei, W.; Wang, D. Nitrogen and sulfur co-doping of 3D hollow-structured carbon spheres as an efficient and stable metal free catalyst for the oxygen reduction reaction. *Nanoscale* **2016**, *8*, 19086–19092. [[CrossRef](#)] [[PubMed](#)]
136. Shu, C.; Song, B.; Wei, X.; Liu, Y.; Tan, Q.; Chong, S.; Chen, Y.; Yang, X.-D.; Yang, W.-H.; Liu, Y. Mesoporous 3D nitrogen-doped yolk-shelled carbon spheres for direct methanol fuel cells with polymer fiber membranes. *Carbon* **2018**, *129*, 613–620. [[CrossRef](#)]
137. Guo, D.; Wei, H.; Chen, X.; Liu, M.; Ding, F.; Yang, Z.; Yang, Y.; Wang, S.; Yang, K.; Huang, S. 3D hierarchical nitrogen-doped carbon nanoflower derived from chitosan for efficient electrocatalytic oxygen reduction and high performance lithium–sulfur batteries. *J. Mater. Chem. A* **2017**, *5*, 18193–18206. [[CrossRef](#)]

